Metabolic reprogramming of hypoxic tumor-associated macrophages through CSF-1R targeting favours treatment efficiency in colorectal cancers

Khaldoun Gharzeddine[1], Cristina Gonzalez Pietro[1], Marie Malier[1], Clara Hennot[1], Renata Grespan[1], Yoshiki Yamaryo-Botté[2], Cyrille Y. Botté[2], Fabienne Thomas[3], Marie-Hélène Laverriere[1,4], Edouard Girard[5], Gael Roth[1,6], Arnaud Millet[1,6]

1. Univ.Grenoble Alpes, Inserm U1209, CNRS UMR5309, Institute for Advanced Biosciences, Team Mechanobiology, Immunity and Cancer, 38000 Grenoble, France

2. Univ.Grenoble Alpes, Inserm U1209, CNRS UMR5309, Institute for Advanced Biosciences, Apicolipid Team & Gemeli metabolomic platform, 38000 Grenoble, France

3. Centre de Recherches en Cancérologie, Inserm, CNRS, Université Toulouse III-Paul Sabatier and IUCT-Oncopole, Toulouse, France.

4. Univ.Grenoble Alpes, CNRS, CHU Grenoble Alpes pathology department, TIMC, 38000 Grenoble, France

5. Univ.Grenoble Alpes, CHU Grenoble Alpes digestive and emergency surgery department, 38000 Grenoble, France

6. Univ.Grenoble Alpes, CHU Grenoble Alpes hepatogastroenterology department, 38000 Grenoble, France

Running title: Metabolic reprogramming of macrophages through CSF-1R targeting

Keywords: CSF-1R antagonists, Cholesterol, Hypoxia, Tumor-Associated Macrophages, Chemoresistance.

Corresponding author: Arnaud Millet MD PhD,

e-mail: arnaud.millet@inserm.fr

Team Mechanobiology, Immunity and Cancer, Institute for Advanced Biosciences

Building Albert Bonniot

Boulevard de la Chantourne

38700 La Tronche

France

The authors declare no conflicts of interest.

Abstract

Tumor-associated macrophages participate in the complex network of support that favors tumor growth. Among the various strategies that have been developed to target these cells, blockade of the CSF-1R receptor is one of the most promising one. Here, we characterize the resulting state of human macrophages exposed to a CSF-1R kinase inhibitor. We find that CSF-1R receptor inhibition in human macrophages is able to impair cholesterol synthesis, fatty acid metabolism and hypoxia-driven expression of dihydropyrimidine dehydrogenase, an enzyme responsible for the 5-fluorouracil macrophage-mediated chemoresistance. We show that this inhibition of the CSF-1R receptor leads to a downregulation of the expression of SREBP2, a transcription factor that controls cholesterol and fatty acid synthesis. We also show that the inhibition of ERK1/2 phosphorylation resulting from targeting the CSF-1R receptor destabilizes the expression of HIF2α in hypoxia resulting in the downregulation of dihydropyrimidine dehydrogenase expression restoring the sensitivity to 5-fluorouracil in colorectal cancer. These results reveal the unexpected metabolic rewiring resulting from the CSF-1R receptor targeting of human macrophages in tumors.

54 **Introduction**

55 A large body of work has been reported providing compelling evidence that tumor-associated
56 macrophages (TAMs) are involved in tumor growth, treatment resistance and metastasis
57 (DeNardo & Ruffell, 2019; Engblom *et al*, 2016). Indeed, TAMs are associated with poor
58 prognosis in the vast majority of solid tumors (Cortese *et al*, 2020). Consequently, great
59 efforts have been made to target TAMs in order to direct the immune response against the
60 tumor (Mantovani *et al*, 2022). CSF-1R is a receptor with intrinsic tyrosine kinase activity that
61 recognizes CSF-1 (M-CSF, macrophage colony stimulating factor) and IL-34. The CSF-1/CSF-1R
62 signaling pathway is involved in macrophage survival, proliferation, differentiation and
63 chemotaxis (Stanley & Chitu, 2014). This pivotal role opens the way to use CSF-1R receptor
64 targeting in various pathological contexts and especially in cancer to modulate macrophages
65 (Cannarile *et al*, 2017). CSF-1R receptor targeting has been used in various tumor mouse
66 models with promising results but only modest beneficial effects in humans when used alone
67 (Mantovani *et al*, 2022). Furthermore, the recognition that the type of tumor model used
68 (O'Brien *et al*, 2021) and the modification of the cellular environment such as oxygen
69 availability (Pradel *et al*, 2016), affect the efficiency of the CSF-1R targeting highlights the
70 need for a better understanding of the functional consequences of CSF-1R receptor targeting
71 on human macrophages.

72 The importance of CSF-1R receptor blockade beyond the induction of apoptosis has been
73 recognized in animal models that advocate the possibility of achieving an anti-tumor
74 phenotypic reprogramming (Pyonteck *et al*, 2013). However, the mechanisms involved in
75 macrophage's reprogramming by CSF-1R targeting are unclear.

76 Here, we characterize the functional consequences of CSF-1R receptor inhibitors on human
77 macrophages. We show that CSF-1R receptor inhibition is associated with impaired
78 cholesterol and fatty acid synthesis under the control of the transcription factor SREBP2.
79 Furthermore, CSF-1R receptor blockade leads to an inhibition of the phosphorylated state of
80 ERK1/2 resulting in a decrease in the expression of HIF2α, a hypoxic response transcription
81 factor. A consequence of the HIF2α-dependent hypoxic response is the downregulation of
82 dihydropyrimidine dehydrogenase expression, the limiting rate enzyme of the first step of the
83 pyrimidine catabolic pathway, which is responsible for a hypoxia-driven macrophage-
84 mediated chemoresistance to 5-fluorouracil in colorectal cancer (Malier *et al*, 2021).

85 **Results**

86 **Complete CSF-1R inhibition is associated with a profound phenotypic change without death**
87 **induction in human macrophages**

88 Upon ligation of CSF-1, the CSF-1 receptor dimerizes, resulting in multiple site
89 phosphorylation of the intracellular tail of the receptor (Stanley & Chitu, 2014). To investigate
90 the resulting effect of inhibition of the CSF-1R receptor-dependent signaling pathway, we first
91 evaluated the response of tyrosine 723 phosphorylation to increasing doses of edicotinib, a
92 selective CSF-1R tyrosine kinase inhibitor (Kumar *et al*, 2017; von Tresckow *et al*, 2015;
93 Genovese *et al*, 2015). We found that edicotinib at 10µM is able to completely inhibit CSF-
94 1R's phosphorylation (Figure 1A). Targeting the CSF-1R receptor with tyrosine kinase
95 inhibitors is a strategy used in mice to deplete macrophages (Ries *et al*, 2014). However, we
96 found that the complete inhibition of CSF-1R phosphorylation in human primary
97 macrophages was not associated with cell death induction (7AAD and Annexin V) (Figure 1B
98 & Supplementary Figure 1) or disruption of cellular metabolic activity (MTT) (Figure 1C). The

99 importance of CSF-1 in macrophage differentiation and polarization prompted us to evaluate
100 the effect of CSF-1R receptor blockade on human macrophage phenotype. To achieve this
101 goal, we performed a global gene expression analysis by RNA sequencing (RNAseq) on bulk
102 macrophages 48h after exposure to vehicle and edicotinib. To extract differentially expressed
103 genes between treated and naïve macrophages, we used a moderated t-test with an adjusted
104 p-value (Benjamini-Hochberg procedure with a threshold set at q-value <0.05) and a fold
105 change threshold set at 2 (log_2 FC <-1 or Log_2 FC > 1). CSF-1R receptor inhibition by edicotinib
106 was associated with 740 downregulated and 481 upregulated genes (Figure 1D). We then
107 used a Gene Ontology (GO) enrichment analysis to identify pathways affected by edicotinib.
108 The GO terms associated with genes downregulated by edicotinib indicated that the
109 regulation of the cholesterol metabolic pathway, the inhibition of the ERK1/2 pathway, and
110 lipid synthesis were the main of biological processes identified as a result of CSF-1R receptor
111 blockade (Figure 1E).

112 **CSF-1/CSF-1R regulates cholesterol synthesis in human macrophages via the transcription**
113 **factor SREBP2**

114 To explore the gene ontology identification of cholesterol synthesis regulation under CSF-1R
115 targeting, we examined the expression of all the enzymes involved in the cholesterol synthesis
116 starting from acetyl-CoA. Cholesterol, an essential lipid component of mammalian cells, is
117 mainly obtained by endogenous synthesis or uptake. Endogenous synthesis relies on nearly
118 30 enzymatic reactions (Nes, 2011). We found that genes coding for enzymes involved in
119 cholesterol synthesis *ACAT2*, *HMGCS1, HMGCR, MVK, PMVK, MVD, IDI1, FDPS, FDFT1, SQLE,*
120 *LSS, CYP15A1, TMF7SF2, NSDHL, HSD17B7, MSMO1, SC5D, EBP, DCHR7, DCHR24* are
121 downregulated under edicotonib exposure (Figure 2A) and except for two of them (*PMVK*,

122 *LSS*) the fold change is greater than 2 (Figure 2B). The control of cholesterol synthesis genes
123 by the CSF-1/CSF-1R pathway was confirmed by the stimulation of human macrophages by
124 CSF-1, which showed the upregulation of *HMGCR* and *DHCR7* (Figure 2C). SREBP2 (Sterol
125 regulatory element-binding protein 2) is a helix-loop-helix leucine zipper transcription factor
126 that regulates the synthesis and cellular uptake of cholesterol (Horton *et al*, 1998). Using the
127 ENCODE data set (The ENCODE (ENCyclopedia Of DNA Elements) Project, 2004), we have
128 explored the known targets of this transcription factor and found that the cholesterol
129 synthesis genes are under the control of SREBP2 (Figure 2D). Interestingly, the LDL receptor
130 (*LDLR*) which is responsible for cellular uptake of cholesterol from the extracellular milieu and
131 the fatty acid synthetase (*FASN*) are also SREBP2 target genes (Figure 2D). We validated the
132 SREBP2 dependent expression of cholesterol synthesis genes (*HMGCR*, *DHRC7*) and *LDLR*
133 using RNAi targeting against SREBF2, the gene encoding the SREBP2 protein (Figure 2E). We
134 demonstrated the control of *SREBF2* by the CSF-1/CSF-1R pathway by showing that *SREBF2*
135 expression is increased under CSF-1 stimulation (Figure 2F) and decreased when CSF-1R is
136 blocked by edicotinib (Figure 2G). We confirmed that the active form of SREBP2 expression is
137 downregulated by the CSF-1R blockade (Figure 2H). In addition, *LDLR*, a target of SREBP2, is
138 downregulated by edicotinib (Figure 2I). We observed the resulting decrease in cellular
139 cholesterol levels under edicotinib exposure similar to what is found using RNAi targeting of
140 SREBF2 or blockade of HMGCR activity with simvastatin, a specific inhibitor (Figure 2J). The
141 cellular homeostasis of cholesterol is a balance between synthesis, uptake and efflux. The
142 impairment of cholesterol synthesis and uptake by CSF-1R receptor blockade could be
143 compensated by a decrease in cholesterol efflux. To evaluate this possibility, we studied the
144 expression of the two major cholesterol efflux transporters expressed in macrophages ABCA1
145 and ABCG1. We found that the CSF-1R targeting did not decrease the expression of these

146 transporters in macrophages (Supplementary Figure 2A) and that the decrease in intracellular
147 cholesterol levels induced by CSF-1R receptor blockade resulted in a global decrease in
148 macrophage cholesterol secretion (Supplementary Figure 2B).

149 **Edicotinib interferes with the macrophage-tumor communication resulting in modulation**
150 **of cholesterol synthesis in colorectal cancers**

151 Membrane cholesterol efflux from macrophages has been reported to be involved in tumor
152 growth (Goossens *et al*, 2019). This efflux relies on the ability of macrophages to express efflux
153 transporters but also on the maintenance of their intracellular cholesterol pool based on
154 synthesis and uptake. To further understand the importance of cholesterol synthesis in the
155 cross-talk between macrophages and tumors, we performed a co-culture between human
156 macrophages and tumor or non-tumor tissues from the same colon obtained from surgical
157 resection of colorectal adenocarcinomas (Figure 2K). We observed that macrophages under
158 the influence of tumor tissue upregulate their cholesterol synthesis genes as well as the
159 cholesterol uptake receptor LDLR under the control of SREBF2 which is upregulated by the
160 tumor (Figure 2L). We also demonstrated that edicotinib is able to counteract this tumor-
161 driven metabolic reprogramming by interfering with cholesterol synthesis and uptake (Figure
162 2L). This communication between tumors and macrophages suggested the involvement of
163 the CSF-1/CSF-1R pathway. We confirmed that tumors secrete significantly more CSF-1 than
164 non-tumor tissues, which drives cholesterol synthesis and uptake in macrophages (Figure
165 2M). Nevertheless, we sought to verify whether edicotinib could also affect the expression of
166 the CSF-1R receptor on the surface of macrophages but found no decrease in receptor
167 following CSF-1R blockade (Figure 2N). Interestingly, we found that the ability of macrophages
168 to produce their own CSF-1 is impaired in human macrophages exposed to edicotinib (Figure

169 2O). Even when tumors do not increase the autocrine-associated production in macrophages,
170 edicotinib is able to downregulate this production in macrophages, enhancing the blockade
171 of the CSF-1/CSF-1R pathway (Figure 2P).

172 **CSF-1R receptor targeting downregulates HIF2α expression in hypoxia through inhibition of**
173 **ERK1/2 phosphorylation**

174 Previous studies have shown that several environmental factors can modulate the cellular
175 response to CSF-1R receptor targeting (Pradel *et al*, 2016). Among these factors, hypoxia is of
176 particular interest because the tumor environment is associated with low oxygen availability
177 (Wilson & Hay, 2011). To assess the interplay between hypoxia and CSF-1R receptor targeting,
178 we performed the study of differentially expressed genes in hypoxia compared to normoxia
179 and analyzed the impact of edicotinib on the hypoxic response (Figure 3A). The cell survival
180 profile of CSF-1R receptor blockade in hypoxia was similar to what we found in normoxia
181 (Supplementary Figure 3A). Heat-map analysis revealed that specific hypoxia-sensitive genes
182 exhibited two distinct patterns: specific hypoxia-sensitive genes that maintained their
183 expression profile under CSF-1R receptor blockade (clusters 1 & 3) and genes with a modified
184 profile under CSF-1R receptor blockade (clusters 2, 4 & 5). Among the hypoxia upregulated
185 genes (cluster 3), we found several genes *LDHA*, *NDRG1*, *P4HA1* and *SLC2A1* (Figure 3B), which
186 are part of the HIF1α target gene set identified by ChIP enrichment analysis (Lachmann *et al*,
187 2010) suggesting that the HIF1α-dependent hypoxic response is mainly independent of the
188 CSF-1R pathway. Of particular interest, we observed that the downregulation of some hypoxic
189 genes is abolished by CSF-1R receptor blockade (cluster 2) with an increased expression
190 profile in normoxia (Figure 3A). One of this gene is *EPAS1* (Figure 3C). The *EPAS1* gene encodes
191 the transcription factor HIF-2α, which plays an essential role in the cellular response to low

192 oxygen environments (McGettrick & O'Neill, 2020). The downregulation of *EPAS1* mRNA in
193 hypoxia contrasts with the stabilization of HIF-2α protein in the same condition (Figure 3D).
194 To understand the role of CSF-1R in the HIF-2α-dependent hypoxic response, we sought to
195 elucidate the function of HIF-2α by studying *FLT1* (VEGFR1), a HIF-2α target gene (Sasagawa
196 *et al*, 2018). Indeed, *FLT1* expression is increased in hypoxic macrophages (Figure 3E) under
197 the control of HIF-2α transcriptional activity, as demonstrated by RNAi targeting of EPAS1 in
198 hypoxic macrophages (Supplementary Figure 3B). The decrease of FLT1 (Figure 3E) and the
199 corresponding increase of EPAS1 mRNA level upon CSF-1R receptor blockade by edicotinib in
200 hypoxic macrophages (Figure 3C) supports a decrease of HIF-2α expression in hypoxia under
201 CSF-1R receptor blockade, a pattern that we confirmed by immunoblot (Figure 3F).
202 Interestingly, the activation of HIF-2α leading to its translocation to the nucleus and fixation
203 on Hypoxic Response Elements (HRE) gene promotors is ERK1/2 dependent (Conrad *et al*,
204 1999). The identification of the ERK1/2 pathway as a target of CSF-1R blockade in normoxia
205 (Figure 1E) suggested the possibility of a similar pattern in hypoxia. Indeed, we confirmed this
206 pattern by a gene set enrichment analysis (GSEA) (Figure 3G) and by immunoblotting of
207 phosphorylated sites p-ERK1/2 sites in hypoxia (Figure 3H). Inhibition of ERK1/2 with the
208 MEK1 inhibitor U0126 was able to downregulate the expression of HIF-2α similar to that
209 observed with edicotinib (Figure 3I). In addition, HIF-2α protein expression is a direct sensor
210 of intracellular oxygen availability. Oxygen diffusion from the cellular environment into the
211 cell is primarily controlled by the plasma membrane permeability which is profoundly affected
212 by the membrane concentration of cholesterol (Dotson *et al*, 2017). A decrease in membrane
213 cholesterol will favor oxygen diffusion into the cell. Therefore, the decrease in cholesterol
214 synthesis induced by CSF1R blockade suggested a complementary involvement of the cellular
215 cholesterol in HIF-2α expression. Indeed, the RNAi targeting of SREBF2, which led to a

216 decrease in cholesterol synthesis and cellular uptake, showed a small decrease in HIF-2α
217 (Figure 3J), suggesting a possible combined effect between SREBF2- and ERK1/2-dependent
218 processes. Examination of the expression of cholesterol synthesis genes (*HMGCR*, *DHCR7*) and
219 cellular uptake (*LDLR*) confirms that these two mechanisms are independent as ERK1/2
220 inhibition did not downregulate these genes, in contrast to edicotinib exposure
221 (Supplementary Figure 3C).

222 **Hypoxia-induced increase in fatty acid synthesis reversed by CSF-1R targeting in human**
223 **macrophages**

224 The recent recognition that hypoxia activates SREBP2 in hypoxic THP1-monocytes raised the
225 possibility that the ability of CSF-1R receptor blockade to dampen cholesterol synthesis could
226 be antagonized in hypoxic macrophages (Nakahara *et al*, 2023). However, these authors
227 reported a small or absent effect in hypoxic differentiated THP1-macrophages (Nakahara *et*
228 *al*, 2023). We sought to address this issue in our primary human macrophages. Examination
229 of differentially repressed genes in exposed hypoxic macrophages confirmed the results
230 obtained in normoxia with a downregulation of the cholesterol synthesis and the ERK1/2
231 pathway under CSF-1R blockade (Figure 4A). In addition to cholesterol synthesis and cellular
232 uptake under the control of *SREBF2*, we observed that *SREBF1* and *FASN* were similarly
233 downregulated in hypoxia under CSF-1R blockade (Figure 4B). SREBP1, the transcription
234 factor encoded by the *SREBF1* gene, is involved in fatty acid synthesis and fatty acid synthase
235 (FASN) is under the control of SREBPs transcription factors. Furthermore, the analysis of the
236 hypoxia-specific response genes modulated by edicotinib (cluster 4 in Figure 3A) revealed that
237 lipid transport, localization is associated with the hypoxia response (Figure 4C), and that this
238 response could be disrupted by CSF-1R blockade. *FASN*, a gene under the control of *SREBF1*

239 and *SREBF2*, is the major enzymatic complex responsible for the synthesis of palmitic acid
240 (C16:0) and stearic acid (C18:0) from malonyl-CoA, which are subsequently converted to
241 palmitoleic acid (C16:1 cis) and oleic acid (C18:1 cis) respectively (Figure 4D). Fatty acids,
242 particularly oleic acid, have been implicated in macrophage commitment to an
243 immunosuppressive $CD206^{+}CD38^{+}$ phenotype in tumor-associated macrophages (Wu *et al*,
244 2019). Using gas chromatography-mass spectrometry (GC-MS), we confirmed the significant
245 increase of these fatty acids in hypoxic macrophages and the ability of the CSF-1R blockade
246 to attenuate this synthesis (Figure 4E). We also confirmed the downregulation of CD206
247 expression in tumor-educated macrophages (Figure 4F & Supplementary Figure 4A) and
248 *CD206*, *CD38* gene expression in hypoxic macrophages exposed to edicotinib (Supplementary
249 Figure 4 B). We also found that inhibition of FASN by a specific inhibitor (C75) in hypoxic
250 macrophages was sufficient to prevent IL-4 driven CD206 expression (Figure 4G). These
251 results support for a fatty acid synthase-mediated inhibition of CD206 following CSF-1R
252 targeting.

253 **CSF-1R targeting downregulates the expression of dihydropyrimidine dehydrogenase**
254 **preventing 5-FU hypoxic macrophage-driven chemoresistance**

255 HIF-2α has been recognized as an important regulator of innate immunity in the context of
256 tumors, in particular by controlling macrophage's recruitment (Imtiyaz *et al*, 2010). In
257 addition, we recently reported that HIF-2α controls the expression of dihydropyrimidine
258 dehydrogenase (DPD) in hypoxia independently of its transcription factor activity. DPD
259 expression in hypoxic macrophages is responsible for a resistance to 5-fluorouracil in human
260 colorectal cancer (Malier *et al*, 2021). We have shown in the same study that rodent models
261 are inadequate to mimic this mechanism, because the DPYD gene is epigenetically negatively

262 regulated in rodent macrophages, in contrast to humans. Downregulation of HIF-2α
263 expression under CSF-1R blockade offers a potential strategy to restore chemosensitivity in
264 this context. Indeed, edicotinib is able to downregulate the expression of DPD in hypoxic
265 macrophages (Figure 5A), resulting in the complete abrogation of its enzymatic activity,
266 preventing the conversion of uracil to dihydrouracil (Figure 5B). We confirmed the inhibition
267 of the HIF-2α-dependent synthesis of DPD during the transition to hypoxia, which requires
268 the continuous destabilization of HIF-2α during the transition (Figure 5C). The previous
269 demonstration that ERK1/2 phosphorylation controls HIF-2α expression implies an expected
270 control of DPD expression in the same context as we confirmed (Figure 5D) as well as the
271 implication of the cellular cholesterol content in the hypoxia-induced DPD expression in
272 macrophages (Figure 5E). Consequently, the downregulation of DPD expression obtained by
273 CSF1R targeting allows the restoration of 5-FU sensitivity of HT-29 and RKO colorectal cancer
274 cells in a co-culture setting (Figure 5F). We have previously shown that DPD expression under
275 the HIF-2α expression is not related to mRNA modulation (Malier *et al*, 2021), to ensure that
276 this is still the case in the tumor environment we showed that edicotinib downregulates DPD
277 expression in hypoxic TAMs co-cultured with tumors (Figure 5G) without downregulating its
278 mRNA as expected (Figure 5H). We have previously shown that macrophages are the major
279 source of DPD expression in colorectal cancer (Malier *et al*, 2021). However, these
280 macrophages are replenished by circulating monocytes and these hypoxic monocytes (CD14+)
281 express DPD in contrast to other immune cells such as hypoxic T (CD3+) or B (CD19+)
282 lymphocytes (Figure 5I & Supplementary Figure 5), representing another source of immune-
283 driven chemoresistance to 5-FU. Circulating monocytes are recruited to tumor sites by
284 CCL2/CCL7 chemokine secretion from tumor macrophages (Qian *et al*, 2011; Sanford *et al*,
285 2013; Yang *et al*, 2020). Edicotinib may interfere with this process. Indeed, the gene ontology

286 – biological process associated with myeloid leukocyte migration was associated with
287 differentially downregulated genes by CSF-1R blockade (Figure 4A). We confirmed this
288 pattern by the effect of CSF-1R targeting on the expression of *CCL2* and *CCL7* in macrophages
289 (Figure 5J). Similarly, CCL2 and CCL7 expressions are disrupted in hypoxic TAMs exposed to
290 edicotinib (Figure 5K). These results demonstrate the ability of CSF-1R targeting to disrupt
291 DPD expression in tumor-associated macrophages and prevent the recruitment of DPD-
292 expressing myeloid cells to the tumor site.

293 **Discussion**

294 Tumor-associated macrophages are an essential component of the tumor immune
295 microenvironment in the vast majority of cancers. Their involvement in angiogenesis,
296 extracellular matrix remodeling, cancer cell proliferation, metastasis spreading and treatment
297 resistance is leading to the development of macrophage-centered therapeutic strategies
298 (Mantovani *et al*, 2022). The importance of the CSF-1/CSF-1R axis in macrophage survival,
299 differentiation and activation makes CSF-1R targeting a favored approach to remodel TAMs.
300 Two strategies have been pursued to achieve this goal: blocking the interaction between the
301 ligand (CSF-1, IL-34) and its receptor using specific anti-CSF-1R antibodies or inhibiting the
302 tyrosine kinase activity of CSF-1R using specific inhibitors. Various inhibitors have been
303 developed over the years, and despite high specificity against CSF-1R, these molecules have
304 failed to show a strong clinical effect when used as monotherapy (El-Gamal *et al*, 2018;
305 Mantovani *et al*, 2022). The unclear reasons for this lack of efficacy led us to design the current
306 study to investigate in detail the molecular consequences of CSF-1R blockade using a selective
307 CSF-1R kinase inhibitor (edicotinib or JNJ40346527), which has already been validated in
308 humans (Genovese *et al*, 2015; von Tresckow *et al*, 2015).

309 We observe a clear metabolic shift in CSF-1R-targeted macrophages, mainly focused on
310 cholesterol and fatty acid metabolism. The link between CSF-1 and cholesterol metabolism
311 was suggested in a previous study (Irvine *et al*, 2009). We confirm the ability of CSF-1 to induce
312 cholesterol synthesis and show that CSF-1R blockade is able to downregulate *SREBF2*
313 expression leading to the inhibition of the cholesterol synthesis but also its cellular uptake.
314 We observe that colorectal tumors favor *SREBF2* expression and consequently drives the
315 increase of cholesterol levels in human macrophages. Cholesterol efflux from macrophages
316 under the control of transporter proteins such as ABCA1/ABCG1 has been associated with
317 tumor growth (Goossens *et al*, 2019). Tumor cells exposed to macrophage-secreted
318 cholesterol secrete hyaluronic acid that drives macrophage reprogramming toward an M2
319 phenotype in mice (Goossens *et al*, 2019). Even if cholesterol transporters are not suppressed
320 in macrophages targeted by edicotinib, the decreased total amount of cellular cholesterol
321 induced by edicotinib prevents the ability of macrophages to maintain their secretion,
322 thereby braking the feedback loop between tumor-associated macrophages and tumors.

323 Since cholesterol is synthesized by the metabolic synthesis starting from acetyl-coA, which is
324 produced by the fatty acid β-oxidation pathway, we investigated the fatty acid synthesis in
325 macrophages. We find that edicotinib is able to prevent the increase in fatty acid
326 accumulation driven by hypoxia in human macrophages (Figure 4E), thereby preventing the
327 appearance of an immunosuppressive phenotype $CD206^{+}CD38^{+}$ induced by oleate
328 (Supplementary Figure 4).

329 The CSF-1R blockade strategy is designed to occur in the low-oxygen tumor environment. The
330 sensitivity of cholesterol synthesis and CSF-1 coupling in hypoxia is not known. A recent study
331 highlighted the importance of hypoxia in the induction of cholesterol synthesis in monocytes

332 but not in differentiated macrophages (Nakahara *et al*, 2023). The influence of CSF-1R
333 targeting on the hypoxic response shows that *EPAS1,* which encodes HIF-2α, is upregulated.
334 In conjunction with this observation, we note the inverse correlation between *EPAS1* mRNA
335 and HIF-2α protein, revealing the counterregulation of *EPAS1* transcription by HIF-2α itself. A
336 similar observation has been proposed for HIF-1α, based on miR-429, whose expression is
337 promoted by HIF-1α (Bartoszewska *et al*, 2015). However, this negative feedback loop was
338 associated with the decrease of HIF-1α in chronic hypoxia. Our observation was made in
339 chronic hypoxia and no decrease of HIF-2α protein was observed. This observation needs to
340 be further investigated to determine the direct or indirect mechanism. Our observation of the
341 association between CSF-1R targeting and HIF-2α expression revealed the role of ERK1/2
342 activation in stabilizing this hypoxia-inducible factor in human macrophages. The
343 downregulation of HIF-2α opens a promising avenue to target the recently identified
344 mechanism leading to the chemoresistance to 5-FU driven by hypoxic macrophages in
345 colorectal cancer (Malier *et al*, 2021). In this study, we show that targeting CSF-1R
346 downregulates ERK1/2 phosphorylation, which in turn prevents HIF-2α expression in hypoxia,
347 thereby preventing the expression of DPD, which can no longer degrade 5-fluorouracil. We
348 further find that monocyte recruitment driven by the CCL2/CCL7 axis is also disrupted,
349 preventing the contribution of other myeloid DPD-expressing cells to tumor infiltration.

350 In this study, we have provided compelling evidence showing that CSF-1R blockade is an
351 effective strategy to prevent cancer cell-driven TAM recruitment and macrophage-induced
352 resistance to chemotherapy. We have demonstrated the efficacy of an inhibitor of CSF-1R
353 kinase activity to achieve metabolic reprogramming of tumor-associated macrophages by
354 interfering with the cholesterol and fatty acid mediated cross-talk between macrophages and
355 cancer cells.

356 **Material and Methods**

357 **Resources**

Reagent or Resource	Source	Reference/RRID
Experimental Model		
HT-29	ATCC	HTB-38 / CVCL_0320
RKO	ATCC	CRL-2577 / CVCL_0504
THP-1	ATCC	TIB-202 / CVCL_0006
Antibodies		
Mouse anti β-Actin monoclonal antibody	Sigma	A2228 / AB_476697
Rabbit anti-human CSF-1R polyclonal antibody	Cell Signaling Technology	3152 / AB_2085233
Rabbit anti-human Phospho-M-CSF Receptor (Tyr723) (49C10) monoclonal antibody	Cell Signaling Technology	3155 / AB_2085229
Mouse anti-DPD monoclonal antibody	Santa Cruz	Sc-271308 / AB_10610363
Rabbit anti-p44/42 MAPK (Erk1/2) (137F5) monoclonal antibody	Cell Signaling Technology	4695 / AB_390779
Rabbit anti- Phospho-p44/42 MAPK (Erk1/2) (Thr202/Tyr204) (D13.14.4E) monoclonal antibody	Cell Signaling Technology	4370 / AB_2315112
Mouse anti-HIF2α monoclonal antibody, unconjugated	Santa Cruz	Sc-46691 / AB_627523
Rabbit Anti-SREBP2 polyclonal antibody, Unconjugated	Abcam	Ab30682 / AB_779079
Anti -human CD14-FITC REAfinity	Miltenyi Biotec	REA599/ AB_2801871
Anti-human CD20-PE REAfinity	Miltenyi Biotec	REA780/ AB_2656072
Mouse Anti-human CD3-APC	BD Pharmingen	555342/ AB_398592
Mouse anti human-CD206	Santa Cruz	Sc-376232 / AB_10989352
STAT6 E10 mouse monoclonal	Santa Cruz	Sc-271213 / AB_10611300
pSTAT6 (pY641.18) mouse monoclonal	Santa Cruz	Sc-136019 / AB_2197371
TGM2 (CUB 7402) mouse monoclonal	Life Technologies	MA512739 / AB_10985077
CD14-FITC, human (REA599)	Miltenyi Biotec	130-110-518/ AB_2655049
CD206-PE, human	Miltenyi Biotec	130-095-220 / AB_10827704
RNA Extraction and RT-qPCR Kits		
iScript Ready-to-use cDNA supermix	Biorad	1708841

iTaq universal SYBR green supermix	Biorad	1725124
NucleoSpin RNA (250)	Macherey Nagel	740955.250
Media and reagents		
5-Fluorouracil (5-FU)	Roche	
β-mercaptoethanol	Sigma	M3148-100ML
Bovine Serum Albumin (BSA) solution 30%	Sigma	A9576-50ML
CD14 microbeads, human	Miltenyi Biotec	130-050-201
CD20 microbeads, human	Miltenyi Biotec	130-091-104
CD3 microbeads, human	Miltenyi Biotec	130-091-043
Human IL4, premium grade	Miltenyi Biotec	130-093-921
Human MCSF, premium grade	Miltenyi Biotec	130-096-489
Chloroform	Sigma	34854
DMSO for cell culture	Dutscher	702631
DPBS (1X) , no calcium, no magnesium	Life Technologies	14190169
Edicotinib	MedChemExpress	HY-109086
EDTA (0.5M), pH 8.0, RNase-free	Life Technologies	AM9260G
Fetal Bovine Serum (FBS), qualified, US	Life Technologies	26140079
HEPES (1M)	Life Technologies	15630056
Histopaque-1077	Sigma	10771-6X100ML
Human serum from male AB plasma (SAB)	Sigma	H4522-100ML
Methanol	Sigma	34860
RPMI 1640 medium, glutaMAX supplement	Life Technologies	61870044
Scyllo Inositol	Sigma	I8132
TrypLE Express Enzyme (1X), phenol red	Life Technologies	12605036
Tridecanoic Acid	Sigma	91988
Triton X-100	Fischer Scientific	85111
U0126	Sigma	662005
C75	Sigma	C5490
Oligonucleotides		
B2M forward	Eurogentec	5’ – GTGCTCGCGCTACTCTCTC – 3’
B2M reverse	Eurogentec	5’ – CGGATGGATGAAACCCAGACA – 3’
DPYD forward	Eurogentec	5’ - CGCAGGACCAGGGGTTTTAT - 3’
DPYD reverse	Eurogentec	5’ - TGGCAATGGAGAGTGACAGG - 3’
HPRT1 forward	Eurogentec	5’ – TGCTTTCCTTGGTCAGGCAG – 3’
HPRT1 reverse	Eurogentec	5’ – TTCGTGGGGTCCTTTTCACC – 3’
SREBF2 forward	Eurogentec	5’ – TGAGCCAGGAAGCCCTCTAT – 3’
SREBF2 reverse	Eurogentec	5’ – CAGAAGAATCCGTGAGCGGT – 3’
HMGCR forward	Eurogentec	5’ – GCTTTGCCCTTTTTCCTACTTTTG – 3’
HMGCR reverse	Eurogentec	5’ – ACCAACTCCAATCACAAGACATTC – 3’
DHCR7 forward	Eurogentec	5’ – GACCCTCATCAACCTGTCCTT – 3’
DHCR7 reverse	Eurogentec	5’ – GCAGATGTCAATGGTCTTCAGG – 3’
LDLR forward	Eurogentec	5’ – TACAAGTGCCAGTGTGAGGAA – 3’
LDLR reverse	Eurogentec	5’ – TTGGTGAAGAAGAGGTAGGCG – 3’
EPAS1 forward	Eurogentec	5‘ – GCAATCAGCTTCCTGCGAAC – 3’

EPAS1 reverse	Eurogentec	5’ – CGGCAATGAAACCCTCCAAG – 3’
FLT1 forward	Eurogentec	5’ – AAAGCCACCAACCAGAAGGG – 3’
FLT1 reverse	Eurogentec	5’ GCCACACAGGTGCATGTTAG – 3’
CCL2 forward	Eurogentec	5’ – AGCAGCAAGTGTCCCAAAGA – 3’
CCL2 reverse	Eurogentec	5’ – TTTGCTTGTCCAGGTGGTCC – 3’
CCL7 forward	Eurogentec	5’ – TGGAGAGCTACAGAAGGACCA – 3’
CCL7 reverse	Eurogentec	5’ – GGGTTTTCTTGTCCAGGTGCT – 3’
CSF-1 forward	Eurogentec	5’ – CAGCAAGAACTGCAACAACAGC – 3’
CSF-1 reverse	Eurogentec	5’ GGTCACTGCTAGGGATGGCT – 3’
CD206 forward	Eurogentec	5’ – CCATCGAGGAAGAGGTTCGG – 3’
CD206 reverse	Eurogentec	5’ – CCTGCAATCCCGGTTCTCAT – 3’
ON-TARGETplus Human SREBF2 (6721) siRNA - SMARTpool, 5 nmol	Dharmacon	L-009549-00-0005
ON-TARGETplus Non-Targeting pool, 5 nmol	Dharmacon	D-001810-10-05
ON-TARGETplus Human EPAS1 (2034) siRNA – SMARTpool, 5 nmol	Dharmacon	L-004814-00-0005
Others		
7-AAD staining solution	BD Biosciences	559925
Annexin V-FITC	Miltenyi Biotec	130-093-060
Cholesterol/Cholesteryl Ester Assay Kit - Quantification	Abcam	Ab65359
Cell Titer 96 Non-radioactive Cell Proliferation Assay (MTT)	Promega	G4000
LS columns	Miltenyi Biotec	130-042-401
Softwares		
Prism v7	GraphPad	
JMP v14	SAS	
Galileo	Integragen	

Human samples

Human blood samples from healthy de-identified donors were obtained from EFS (French national blood service) as part of an authorized protocol (CODECOH DC-2018–3114). Donors gave signed consent for use of their blood in this study. Tumorous and non tumorous tissues were obtained from surgically resected colons at the university hospital of Grenoble Alpes from patients included in the CRC-ORGA2 clinical trial (clinicaltrial.gov, NCT05038358).

365 Inclusion criteria comprise adult patients suffering from colorectal adenocarcinoma treated
366 by surgery without neoadjuvant chemotherapy (Table).

367 **Cell culture**

368 THP-1, RKO and HT-29, were purchased from ATCC. THP-1, HT-29 and RKO were maintained
369 in RPMI (Gibco) supplemented with 10% FBS (Gibco) at 37°C. All cells were routinely tested
370 for mycoplasma contamination using MycoAlert detection kit (Lonza).

371 **Human macrophage differentiation from monocytes**

372 Monocytes were isolated from leukoreduction system chambers of healthy EFS donors using
373 differential centrifugation (Histopaque 1077, Sigma) to obtain PBMCs. $CD14^+$ microbeads
374 (Miltenyi Biotec) were used to select monocytes according to the manufacturer's instructions.
375 Monocytes were plated in RPMI (Life Technologies) supplemented with 10% SAB (Sigma), 10
376 mM HEPES (Life Technologies), MEM Non-essential amino acids (Life Technologies) and 25
377 ng/mL M-CSF (Miltenyi Biotec). Differentiation was obtained after 6 days of culture. Hypoxic
378 cultures were performed in a hypoxic chamber authorizing an oxygen partial pressure control
379 (HypoxyLab, Oxford Optronix, UK). Hypoxia experiments were performed at 25 mmHg of
380 oxygen (~ 3%). $CD3^+$ T lymphocytes and $CD20^+$ B lymphocytes were sorted from PBMCs using
381 $CD3^+$ and $CD20^+$ microbeads (Miltenyi Biotec) according to the manufacturer's instructions.

382 **Preparation of tumor associated macrophages**

383 Tumorous and non-tumorous tissues obtained from colon of CRC patients. Tissues were kept
384 and transported in ice in RPMI medium supplemented with non-essential amino acids and
385 HEPES as well as antibiotics including penicillin-streptomycin and gentamicin and antifungal
386 amphotericin B. Tissues were minced in pieces of 2-4 mm^3 and deposited on cell culture

387 inserts (4 pieces by insert). These inserts were deposited in 6 well plates on 2 mL of RPMI +
388 10% human serum for 24 h. The resulting medium produced by tumorous and non-tumorous
389 tissues was then used to culture human monocyte derived macrophages for 48h to obtain
390 tumor-associated macrophages.

391 **Macrophage Conditioned Medium (MCM)**

392 THP1 macrophages were plated (12-wells plates) and differentiated at 500,000 cells with
393 50nM of PMA for 24 hours. THP1 macrophages were cultured at 3% oxygen and treated with
394 Edicotinib at 3µM or DMSO acting as a vehicle for 48 hours. Then 1µg/mL of 5-FU was used
395 to generate the 5FU Edicotinib MCM or 5FU Vehicle MCM during 24h. MCM was added for
396 48 hours to two distinct colon cancer cell lines, RKO and HT-29 cells, which were plated
397 previously at 100,000 cells per well (12-wells plates) for 24 hours. Then cancerous cells were
398 collected and counted and the percentage of growth inhibition was assessed for each
399 condition.

400 **RNAseq**

401 RNA extraction was performed using the NucleoSpin RNA kit components (Macherey Nagel)
402 according to the manufacturer's instructions. RNA sequencing was performed using an
403 Illumina HiSeq 4000 sequencer (Integragen). Gene expression quantification was performed
404 using the STAR software. STAR obtains the number of reads associated to each gene in the
405 Gencode v31 annotation (restricted to protein-coding genes, antisense and lincRNAs). Raw
406 counts for each sample were imported into R statistical software. Extracted count matrix was
407 normalized for library size and coding length of genes to compute FPKM expression levels.
408 The Bioconductor edgeR package was used to import raw counts into R statistical software.
409 Differential expression analysis was performed using the Bioconductor limma package and

410 the voom transformation. Gene ontology analysis was performed using the GONet software
411 (https://tools.dice-database.org/GOnet/). Gene list from the differential analysis was ordered
412 by decreasing log2 fold change. Gene set enrichment analysis (GSEA) was performed by
413 clusterProfiler::GSEA function using the fgsea algorithm.

414 **Lipidomics**

415 Human macrophages were metabolically quenched in dry ice – ethanol for one minute then
416 washed three times in cold PBS. Then total lipids were extracted in
417 chloroform/methanol/water (1:3:1, v/v/v) containing PC (C13:0/C13:0), 10 nmol and C21:0
418 (10 nmol) as internal standards for extraction) for 1 h at 4◦C, with periodic sonication. Then
419 polar and apolar metabolites were separated by phase partitioning by adding chloroform and
420 water to give the ratio of Chloroform/Methanol/Water, 2:1:0.8 (v/v/v). For lipid analysis, the
421 organic phase was dried under N2 gas and dissolved in 1-butanol to obtain1µl butanol/10^7
422 macrophages.

423 *Total lipid analysis* – Total lipid was then added with 1 nmol pentadecanoic acid (C15:0) as
424 internal standard and derivatized to give fatty acid methyl ester (FAME) using
425 trimethylsulfonium hydroxide (TMSH, Machenery Nagel) for total glycerolipid content.
426 Resultant FAMEs were then analysed by GC-MS as previously described (Dubois *et al*, 2018).
427 All FAME were identified by comparison of retention time and mass spectra from GC-MS with
428 authentic chemical standards. The concentration of FAMEs was quantified after initial
429 normalization to different internal standards and finally to macrophage number.

430 **Immunoblotting**

431 Cells were lyzed in RIPA buffer supplemented with protease inhibitors (AEBSF 4 mM,
432 Pepstatine A 1 µM and Leupeptin 0.4 mM; Sigma Aldrich) and HIF-hydroxylase inhibitor
433 (DMOG 1 mM, Sigma Aldrich) for total lysate or direct lysis in Laemmli buffer (2X). Proteins
434 were quantified by BCA assay (ThermoFischer) and 15 µg of total protein were run on SDS-
435 PAGE gels. Proteins were transferred from SDS-PAGE gels to PVDF membrane (Biorad),
436 blocked with TBS-Tween supplemented with 5% milk, primary antibodies were incubated at
437 1 µg/mL overnight 4°C. After washing with TBS, the membrane was incubated with a
438 horseradish peroxidase-conjugated secondary antibody (Jackson Immunoresearch). Signal
439 was detected by chemoluminescence (Fusion FX imaging system, Vilber) after exposition to
440 Clarity ECL substrate (Biorad).

441 **Flow cytometry**

442 Flow cytometry data was acquired on an Accuri C6 (BD) flow cytometer. Doublet cells were
443 gated out by comparing forward scatter signal height (FSC-H) and area (FSC-A). At least 10,000
444 events were collected in the analysis gate. Median fluorescence intensity (MFI) was
445 determined using Accuri C6 software (BD).

446 **DPD activity measurements**

447 These analyses were performed in the Pharmacology Laboratory of Institut Claudius-Regaud
448 (France) using an HPLC system composed of Alliance 2695 and diode array detector 2996
449 (Waters). Uracil (U), Dihydrouracil (UH2), Ammonium sulfate 99%, Acetonitrile (ACN) gradient
450 chromasolv for HPLC and 2-propanol were purchased from Sigma. Ethyl acetate Scharlau was
451 of HPLC grade and purchased from ICS (Lapeyrouse-Fossat, France). Water from Milli-Q
452 Advantage A10 and MultiScreen-HV 96-well Plates were used (Merck Millipore). Calibration

453 ranges were 3.125 – 200 ng/mL for U and 25 - 500 ng/mL for UH2 and 5-FU (5µg/mL) was
454 used as an internal standard.

455 **RNA isolation and qPCR analysis for gene expression**

456 Cells were directly lyzed and RNA was extracted using the NucleoSpin RNA kit components
457 (Macherey Nagel) according to the manufacturer's instructions. Reverse transcription was
458 performed using the iScript Ready-to-use cDNA supermix components (Biorad). qPCR was
459 then performed with the iTaq universal SYBR green supermix components (Biorad) on a CFX96
460 (Biorad). Quantification was performed using the ΔΔCt method using two different
461 housekeeping genes.

462 **Quantification of Cholesterol**

463 Macrophages were treated with 10 µM of Edicotinib or Simvastatin for 72 hours afterwhich
464 cells and supernatants were retrieved. Supernatants were stored at -80°C. Lipids were
465 extracted from cells using choloroform:isopropanol:NP-40 (7:11:0.1). Organic phase was
466 taken and air-dried at 50°C and stored at -80°C. The amount of cholesterol in cells and
467 supernatants was assessed using the cholesterol/cholesteryl ester assay quantification kit
468 (ab65359, abcam) according to the manufacturer's instructions.

469 **Silencing of EPAS1 and SREBF2**

470 Fully differentiated macrophages were transfected with siEPAS1 (L-004814-00-0005,
471 Dharmacon) or siSREBF2 (L-009549-00-0005, Dharmacon) at a final concentration of 5nmol/L
472 using Lipofectamine (RNAiMAx, Life Technologies).

473 **Statistical analysis**

Statistics were performed using Graph Pad Prism 7 (Graph Pad Software Inc). When two groups were compared, we used a paired or unpaired two-tailed student's t-test when appropriate. When more than two groups were compared, we used a one-way ANOVA analysis with Sidak's multiple comparison test on paired data when appropriate. The likelihood of data according to a null-hypothesis (p-value) is presented in the figures. The number of independent experiments used to generate the data is shown on each figure.

Data Availability

The data generated and analyzed will be made from the corresponding author on reasonable request.

Acknowledgments

KG has been supported by the ITN (International Training Network) Phys2Biomed project, which was funded from the European Union's Horizon 2020 research and innovation programme under the Marie Skłodowska-Curie grant agreement No 812772 and is supported by the ERiCAN program of Fondation MSD-Avenir (Reference DS-2018-0015). CGP is supported by the Innovative Research Initiative (IRGA 2022) of the university Grenoble Alpes. MM is supported by the APMC Fondation (Agir pour les Maladies Chroniques). This work is supported by the Ligue Régionale contre le Cancer. CYB, and YYB are supported by Agence Nationale de la Recherche, France (Project ApicoLipiAdapt grant ANR-21-CE44-0010 ; Project Apicolipidtraffic grant ANR-23-CE15-0009-01), The Fondation pour la Recherche Médicale (FRM EQU202103012700), Laboratoire d'Excellence Parafrap, France (grant ANR-11-LABX-0024), LIA-IRP CNRS Program (Apicolipid project), the Université Grenoble Alpes (IDEX ISP Apicolipid) and Région Auvergne Rhone-Alpes for the lipidomics analyses platform (Grant IRICE Project GEMELI), Collaborative Research Program Grant CEFIPRA (Project 6003-1) by the

CEFIPRA (MESRI-DBT). We thank Malika Yakoubi for her technical support on DPD chromatographic activity measurment. We thank Dr Lemoigne, Dr Federspiel and Dr Plasse from the University Hospital of Grenoble-Alpes for kindly providing clinical grade 5-Fluorouracil.

Contributions

KG, CGP, MM, CH, RG, AM performed experiments and analysed the data. AM supervised the data analysis. FT performed chromatography measurements. YB, CB performed the lipidomics analysis. GR, EG recruited patients. MHL performed the pathological analysis. AM wrote the original draft and all authors were involved in manuscript editing. Funding acquisition and supervision of the study was performed by AM.

References

Bartoszewska S, Rochan K, Piotrowski A, Kamysz W, Ochocka RJ, Collawn JF & Bartoszewski R (2015) The hypoxia-inducible miR-429 regulates hypoxia-inducible factor-1α expression in human endothelial cells through a negative feedback loop. *FASEB J* 29: 1467–1479

Cannarile MA, Weisser M, Jacob W, Jegg A-M, Ries CH & Rüttinger D (2017) Colony-stimulating factor 1 receptor (CSF1R) inhibitors in cancer therapy. *J Immunother Cancer* 5: 53

Conrad PW, Freeman TL, Beitner-Johnson D & Millhorn DE (1999) EPAS1 trans-Activation during Hypoxia Requires p42/p44 MAPK*. *J Biol Chem* 274: 33709–33713

Cortese N, Carriero R, Laghi L, Mantovani A & Marchesi F (2020) Prognostic significance of tumor-associated macrophages: past, present and future. *Semin Immunol* 48: 101408

DeNardo DG & Ruffell B (2019) Macrophages as regulators of tumor immunity and immunotherapy. *Nat Rev Immunol* 19: 369–382

Dotson RJ, Smith CR, Bueche K, Angles G & Pias SC (2017) Influence of Cholesterol on the Oxygen Permeability of Membranes: Insight from Atomistic Simulations. *Biophys J* 112: 2336–2347

Dubois D, Fernandes S, Amiar S, Dass S, Katris NJ, Botté CY & Yamaryo-Botté Y (2018) Toxoplasma gondii acetyl-CoA synthetase is involved in fatty acid elongation (of long fatty acid chains) during tachyzoite life stages. *J Lipid Res* 59: 994–1004

El-Gamal MI, Al-Ameen SK, Al-Koumi DM, Hamad MG, Jalal NA & Oh C-H (2018) Recent Advances of Colony-Stimulating Factor-1 Receptor (CSF-1R) Kinase and Its Inhibitors. *J Med Chem* 61: 5450–5466

527 Engblom C, Pfirschke C & Pittet MJ (2016) The role of myeloid cells in cancer therapies. *Nat Rev*
528 *Cancer* 16: 447–462

529 Genovese MC, Hsia E, Belkowski SM, Chien C, Masterson T, Thurmond RL, Manthey CL, Yan X
530 (David), Ge T, Franks C, *et al* (2015) Results from a Phase IIA Parallel Group Study of JNJ-
531 40346527, an Oral CSF-1R Inhibitor, in Patients with Active Rheumatoid Arthritis despite
532 Disease-modifying Antirheumatic Drug Therapy. *J Rheumatol* 42: 1752–1760

533 Goossens P, Rodriguez-Vita J, Etzerodt A, Masse M, Rastoin O, Gouirand V, Ulas T, Papantonopoulou
534 O, Van Eck M, Auphan-Anezin N, *et al* (2019) Membrane Cholesterol Efflux Drives Tumor-
535 Associated Macrophage Reprogramming and Tumor Progression. *Cell Metab* 29: 1376–
536 1389.e4

537 Horton JD, Shimomura I, Brown MS, Hammer RE, Goldstein JL & Shimano H (1998) Activation of
538 cholesterol synthesis in preference to fatty acid synthesis in liver and adipose tissue of
539 transgenic mice overproducing sterol regulatory element-binding protein-2. *J Clin Invest* 101:
540 2331–2339

541 Imtiyaz HZ, Williams EP, Hickey MM, Patel SA, Durham AC, Yuan L-J, Hammond R, Gimotty PA, Keith
542 B & Simon MC (2010) Hypoxia-inducible factor 2α regulates macrophage function in mouse
543 models of acute and tumor inflammation. *J Clin Invest* 120: 2699–2714

544 Irvine KM, Andrews MR, Fernandez-Rojo MA, Schroder K, Burns CJ, Su S, Wilks AF, Parton RG, Hume
545 DA & Sweet MJ (2009) Colony-stimulating factor-1 (CSF-1) delivers a proatherogenic signal to
546 human macrophages. *J Leukoc Biol* 85: 278–288

547 Kumar V, Donthireddy L, Marvel D, Condamine T, Wang F, Lavilla-Alonso S, Hashimoto A, Vonteddu
548 P, Behera R, Goins MA, *et al* (2017) Cancer-Associated Fibroblasts Neutralize the Anti-tumor
549 Effect of CSF1 Receptor Blockade by Inducing PMN-MDSC Infiltration of Tumors. *Cancer Cell*
550 32: 654–668.e5

551 Lachmann A, Xu H, Krishnan J, Berger SI, Mazloom AR & Ma'ayan A (2010) ChEA: transcription factor
552 regulation inferred from integrating genome-wide ChIP-X experiments. *Bioinformatics* 26:
553 2438–2444

554 Malier M, Gharzeddine K, Laverriere M-H, Marsili S, Thomas F, Decaens T, Roth G & Millet A (2021)
555 Hypoxia Drives Dihydropyrimidine Dehydrogenase Expression in Macrophages and Confers
556 Chemoresistance in Colorectal Cancer. *Cancer Res* 81: 5963–5976

557 Mantovani A, Allavena P, Marchesi F & Garlanda C (2022) Macrophages as tools and targets in
558 cancer therapy. *Nat Rev Drug Discov*: 1–22

559 McGettrick AF & O'Neill LAJ (2020) The Role of HIF in Immunity and Inflammation. *Cell Metab* 32:
560 524–536

561 Nakahara R, Aki S, Sugaya M, Hirose H, Kato M, Maeda K, Sakamoto DM, Kojima Y, Nishida M, Ando
562 R, *et al* (2023) Hypoxia activates SREBP2 through Golgi disassembly in bone marrow-derived
563 monocytes for enhanced tumor growth. *EMBO J* n/a: e114032

564 Nes WD (2011) Biosynthesis of Cholesterol and Other Sterols. *Chem Rev* 111: 6423–6451

565 O'Brien SA, Orf J, Skrzypczynska KM, Tan H, Kim J, DeVoss J, Belmontes B & Egen JG (2021) Activity of
566 tumor-associated macrophage depletion by CSF1R blockade is highly dependent on the
567 tumor model and timing of treatment. *Cancer Immunol Immunother* 70: 2401–2410

568 Pradel LP, Ooi C-H, Romagnoli S, Cannarile MA, Sade H, Rüttinger D & Ries CH (2016) Macrophage
569 Susceptibility to Emactuzumab (RG7155) Treatment. *Mol Cancer Ther* 15: 3077–3086

570 Pyonteck SM, Akkari L, Schuhmacher AJ, Bowman RL, Sevenich L, Quail DF, Olson OC, Quick ML, Huse
571 JT, Teijeiro V, *et al* (2013) CSF-1R inhibition alters macrophage polarization and blocks glioma
572 progression. *Nat Med* 19: 1264–1272

573 Qian B-Z, Li J, Zhang H, Kitamura T, Zhang J, Campion LR, Kaiser EA, Snyder LA & Pollard JW (2011)
574 CCL2 recruits inflammatory monocytes to facilitate breast-tumor metastasis. *Nature* 475:
575 222–225

576 Ries CH, Cannarile MA, Hoves S, Benz J, Wartha K, Runza V, Rey-Giraud F, Pradel LP, Feuerhake F,
577 Klaman I, *et al* (2014) Targeting Tumor-Associated Macrophages with Anti-CSF-1R Antibody
578 Reveals a Strategy for Cancer Therapy. *Cancer Cell* 25: 846–859

579 Sanford DE, Belt BA, Panni RZ, Mayer A, Deshpande AD, Carpenter D, Mitchem JB, Plambeck-Suess
580 SM, Worley LA, Goetz BD, *et al* (2013) Inflammatory Monocyte Mobilization Decreases
581 Patient Survival in Pancreatic Cancer: A Role for Targeting the CCL2/CCR2 Axis. *Clin Cancer*
582 *Res* 19: 3404–3415

583 Sasagawa T, Nagamatsu T, Morita K, Mimura N, Iriyama T, Fujii T & Shibuya M (2018) HIF-2α, but not
584 HIF-1α, mediates hypoxia-induced up-regulation of Flt-1 gene expression in placental
585 trophoblasts. *Sci Rep* 8: 1–12

586 Stanley ER & Chitu V (2014) CSF-1 Receptor Signaling in Myeloid Cells. *Cold Spring Harb Perspect Biol*
587 6: a021857

588 The ENCODE (ENCyclopedia Of DNA Elements) Project (2004) *Science*

589 von Tresckow B, Morschhauser F, Ribrag V, Topp MS, Chien C, Seetharam S, Aquino R, Kotoulek S, de
590 Boer CJ & Engert A (2015) An Open-Label, Multicenter, Phase I/II Study of JNJ-40346527, a
591 CSF-1R Inhibitor, in Patients with Relapsed or Refractory Hodgkin Lymphoma. *Clin Cancer*
592 *Res* 21: 1843–1850

593 Wilson WR & Hay MP (2011) Targeting hypoxia in cancer therapy. *Nat Rev Cancer* 11: 393–410

594 Wu H, Han Y, Rodriguez Sillke Y, Deng H, Siddiqui S, Treese C, Schmidt F, Friedrich M, Keye J, Wan J,
595 *et al* (2019) Lipid droplet-dependent fatty acid metabolism controls the immune suppressive
596 phenotype of tumor-associated macrophages. *EMBO Mol Med* 11: e10698

597 Yang H, Zhang Q, Xu M, Wang L, Chen X, Feng Y, Li Y, Zhang X, Cui W & Jia X (2020) CCL2-CCR2 axis
598 recruits tumor associated macrophages to induce immune evasion through PD-1 signaling in
599 esophageal carcinogenesis. *Mol Cancer* 19: 1–14

600

601 Figures Legends

602 Figure 1. **Complete CSF-1R inhibition is associated with a profound phenotypic change**.

603 (A) Immunoblot of phosphorylated CSF-1R at site Tyrosine 723, CSF-1R total protein and β-
604 actin (upper panel). Quantification of the level of phosphorylation normalised to β-actin from
605 three independent experiments.

606 (B) Flow cytometry analysis of 7-AAD+ cells treated for 48h. Each condition has its own vehicle
607 control (DMSO) at the same concentration than edicotinib (Ed) (n=3).

608 (C) MTT assay on cells exposed to Edicotinib for 48h (n=3).

609 (D) Volcano-plot analysis of differentially expressed genes between edicotinib vs vehicle
610 (n=4).

611 (E) GO (Gene Ontology)-term analysis of biological processes associated with downregulated
612 genes under edicotinib exposure. Number of genes associated with each GO-terms are
613 indicated.

614 Figure 2. **CSF-1/CSF-1R controls cholesterol synthesis in human tumor-associated**
615 **macrophages**

616 (A) Gene expression of cholesterol synthesis enzymes in human macrophages treated by
617 edicotinib (in red) compared to controls (vehicle in black) (n=4). Gene expression levels are
618 expressed in FPKM=Fragments Per Kilobase Million.

619 (B) The cholesterol synthesis pathway with intermediate products. Enzymes which present a
620 downregulation with a fold change >2 are represented in red.

621 (C) Expression of *HMGCR* and *DHRC7* genes after 6h stimulation by CSF-1 50 ng/mL on
622 previously starved human macrophages determinded by RT-qCPR (n=3).

623 (D) Representation of SREBP2 target genes based on ChIP analysis (ENCODE study).

624 (E) Expression of *SREBF2*, *HMGCR*, *DHCR7* and *LDLR* genes in RNAi treated macrophages
625 against *SREBF2* determined by RT-qPCR (n=5).

626 (F) Expression of *SREBF2* gene after 6h stimulation by CSF-1 50 ng/mL on previously starved
627 human macrophages determinded by RT-qCPR (n=3).

628 (G) Gene expression of *SREBF2* in human macrophages treated by edicotinib (n=4). Gene
629 expression levels are expressed in FPKM=Fragments Per Kilobase Million.

630 (H) Representative immunoblot of mature SREBP2 in human macrophages treated with
631 edicotinib compared to controls (Left panel) using actin as a control loading. Quantification
632 of SREBP2 normalized to the control loading is represented in the right panel (n=3).

633 (I) Gene expression of *LDLR* in human macrophages treated by edicotinib (n=4). Gene
634 expression levels are expressed in FPKM=Fragments Per Kilobase Million.

635 (J) Quantification of intracellular cholesterol in macrophages treated by edicotinib or
636 simvastatin and in RNAi against SREBF2 treated macrophages compared to vehicle (DMSO) or
637 RNAi control respectively (n=3). The amount of decrease is represented in % of the
638 appropriate control (DMSO for Edicotinib and simvastatin; siCTRL for SiSREBF2).

639 (K) Macroscopic view of a colon adenocarcinoma and HES staining of tumorous and non-
640 tumorous tissues used in a co-culture with human macrophages.

641 (L) Expression of *SREBF2*, *HMGCR*, *DHCR7* and *LDLR* genes in hypoxic macrophages cultured
642 with non tumorous and tumorous tissues determined by RT-qPCR (n=5). Tumor associated
643 macrophages were also treated by edicotinib. Relative expression compared to control
644 macrophages in normoxia.

645 (M) ELISA quantification of IL-34 and CSF-1 secreted by tumorous and non-tumorous tissues
646 (n=4).

647 (N) Flow cytometry quantification of membrane CSF-1R expression on macrophages treated
648 by edicotinib compared to controls (DMSO) (n=3).

649 (O) Gene expression of *CSF-1* in human macrophages treated by edicotinib (n=4). Gene
650 expression levels are expressed in FPKM=Fragments Per Kilobase Million.

651 (P) Expression of *CSF-1* gene in hypoxic macrophages cultured with non tumorous and
652 tumorous tissues determined by RT-qPCR (n=4). Tumor associated macrophages were also
653 treated by edicotinib. Relative expression compared to control macrophages in normoxia.

654 Figure 3. **CSF-1R targeting downregulates HIF2α expression in hypoxia through inhibition of**
655 **ERK1/2 phosphorylation.**

656 (A) Hierarchical clustering (Ward methodology) of hypoxic responsive genes (log_2 FC <-1 and
657 log_2 FC >-1 and q-value < 0.05) for normoxic and hypoxic macrophages exposed to edicotinib
658 and vehicle (DMSO).

659 (B) Gene expression of *LDHA, NDRG1, P4HA1* and *SLC2A1* genes in normoxic and hypoxic
660 human macrophages treated by edicotinib or vehicle (n=4). Gene expression levels are
661 expressed in FPKM=Fragments Per Kilobase Million. Normoxia is in blue and hypoxia is in red.

662 (C) Gene expression of *EPAS1* gene in normoxic and hypoxic human macrophages treated by
663 edicotinib or vehicle (n=4). Gene expression levels are expressed in FPKM=Fragments Per
664 Kilobase Million. Normoxia is in blue and hypoxia is in red.

665 (D) Immunoblot of HIF-2α in normoxic and hypoxic macrophages (Representative of five
666 independent experiments).

667 (E) Gene expression of *FLT1* gene in normoxic and hypoxic human macrophages treated by
668 edicotinib or vehicle (n=4). Gene expression levels are expressed in FPKM=Fragments Per
669 Kilobase Million. Normoxia is in blue and hypoxia is in red.

670 (F) Immunoblot of HIF-2α in normoxic and hypoxic macrophages treated by vehicle or
671 edicotinib with a representative experiment (left panel) and quantification of the expression
672 of HIF-2α compared to βactin (right panel) (n=4).

673 (G) Gene Set Enrichment Analysis of the Gene Ontology – Biological Process ERK1 and ERK2
674 cascade for hypoxic macrophages treated by edicotinib.

675 (H) Immunoblot of phosphorylated ERK1/2, total ERK1/2 and βactin in edicotinib treated
676 macrophages (Representative of three independent experiments).

677 (I) Immunoblot of HIF-2α in normoxic and hypoxic macrophages treated by vehicle, edicotinib
678 or U0126 (10µM) with a representative experiment (left panel) and quantification of the
679 expression of HIF-2α compared to βactin (right panel) (n=3).

680 (J) Immunoblot of HIF-2α in normoxic and hypoxic macrophages treated by siRNA against
681 SREBF2 or using siRNA scrambled with a representative experiment (left panel) and
682 quantification of the expression of HIF-2α compared to βactin (right panel) (n=3).

683 Figure 4. **Fatty acid synthesis in hypoxia is reversed by targeting CSF-1R.**

684 (A) GO (Gene Ontology)-term analysis of biological processes associated with downregulated
685 genes under edicotinib exposure in hypoxia. Number of genes associated with each GO-terms
686 are indicated.

687 (B) Heat map of cholesterol synthesis genes associated with *SREBF1*, *FASN* and *SREBF2* for
688 hypoxic macrophages treated by edicotinib compared to vehicle.

689 (C) GO (Gene Ontology)-term analysis of biological processes associated with genes identified
690 in cluster 4 of figure 3A. Number of genes associated with each GO-terms are indicated.

691 (D) Fatty acid synthesis pathway involving the fatty acid synthetase (FASN).

692 (E) Quantification by GS-MS of palmitic acid (C16:0), stearic acid (C18:0), palmitoleic acid
693 (C16:1 cis) and oleic acid (C18:1 cis) in macrophages in normoxia, in hypoxia and in hypoxia
694 treated by edicotinib (n=4).

695 (F) Quantification by flow cytometry of CD206 membrane expression in co-cultured
696 macrophages with RKO cells and IL-4 (25 ng/mL) for 48 h with vehicle (DMSO) or edicotinib
697 (n=3). Representative panel on the left and quantification on the right.

698 (G) Expression of *CD206 (MRC1)* gene in hypoxic macrophages stimulated by IL-4 for 4 hours
699 and a specific inhibitor of FASN (C75 50 µM) determined by RT-qPCR (n=3).

700 Figure 5. **CSF-1R targeting downregulates dihydropyrimidine dehydrogenase expression in**
701 **tumor-associated macrophages**

702 (A) Immunoblot of DPD in normoxic and hypoxic macrophages treated by vehicle (DMSO) and
703 edicotinib with a representative experiment (upper panel) and quantification of the
704 expression of HIF-2α compared to βactin (lower panel) (n=4).

705 (B) Quantification of the reductive activity of DPD through the conversion of uracil (U) to
706 dihydrouracil (UH_2) (n=4).

707 (C) Immunoblot of HIF-2α, DPD and βactin for macrophages treated by edicotinib for 48h then
708 submitted to 6h hypoxia with or without maintaining the CSF-1R blockade (+6h condition).
709 Representative of three independent experiments.

710 (D) Immunoblot of DPD and βactin for macrophages treated by edicotinib or U0126 for 48h
711 then submitted to 6h hypoxia with edicotinib or U0126. A representative experiment is shown
712 in the upper panel and the quantification compared to βactin appears in the lower panel
713 (n=3).

714 (E) Immunoblot of DPD and βactin for macrophages treated by siRNA against SREBF2 or SiRNA
715 scrambled for 48h then submitted to 6h hypoxia. A representative experiment is shown in the
716 upper panel and the quantification compared to βactin appears in the lower panel (n=3).

717 (F) Co-culture between colorectal cancers cells (HT-29, RKO) with human THP1-macrophages.
718 5-FU was used at 1µg/mL for 48h. Edicotinib (5µM) or vehicle (DMSO) was added during 48h
719 (n=3).

720 (G) Immunoblot of DPD and β-actin in hypoxic tumor associated macrophages treated by
721 edicotinib or vehicle (DMSO) (representative of three experiments).

722 (H) Expression of *DPYD* gene in hypoxic macrophages cultured with non-tumorous and
723 tumorous tissues determined by RT-qPCR. Tumor associated macrophages were also treated
724 by edicotinib (n=5). Relative expression compared to control macrophages in normoxia.

725 (I) Immunoblot of DPD and β-actin in CD14+ monocytes, CD3+ T lymphocytes and CD20+ B
726 lymphocytes (representative of three independent healthy donors).

727 (J) Gene expression of *CCL2* and *CCL7* in hypoxic human macrophages treated by edicotinib
728 (n=4). Gene expression levels are expressed in FPKM=Fragments Per Kilobase Million.

729 (K) Expression of *CCL2* and *CCL7* genes in hypoxic macrophages cultured with non-tumorous
730 and tumorous tissues determined by RT-qPCR (n=5). Tumor associated macrophages were
731 also treated by edicotinib. Relative expression compared to control macrophages in
732 normoxia.

733 (L) Schematics of CSF-1 controlled tumor associated macrophages involvement in tumor
734 growth and consequences of CSF-1R targeting. Figure created using Biorender
735 (biorender.com)

736

737 **Supplementary Figure Legends**

738 Supplementary Figure 1

739 Flow cytometry analysis of Annexin-V+ cells treated for 48h. Each condition has its own
740 vehicle control (DMSO) at the same concentration than edicotinib (Ed) (n=3).

741 Supplementary Figure 2

742 (A) Gene expression of *ABCA1* and *ABCG1* genes in human macrophages treated by edicotinib
743 (n=4). Gene expression levels are expressed in FPKM=Fragments Per Kilobase Million.

744 (B) Quantification of extracellular cholesterol secreted by macrophages treated by edicotinib
745 or simvastatin compared to vehicle (DMSO) (n=3). The amount of decrease is represented in
746 % compared to the control.

747 Supplementary Figure 3

748 (A) Flow cytometry analysis of Annexin-V+ cells treated for 48h in hypoxia. Each condition has
749 its own vehicle control (DMSO) at the same concentration than edicotinib (Ed) (n=3).

750 (B) Immunoblot of HIF-2α in macrophages in hypoxia (6h) treated by siRNA against SREBF2 or
751 using siRNA scrambled compared to normoxia (representative of three independent
752 experiments, left panel). Expression of *FLT1* gene after 6h in hypoxia in the same macrophages
753 than in the left panel determined by RT-qCPR (right panel) (n=3).

754 (C) Expression of *HMGCR*, *DHCR7* and *LDLR* genes in hypoxic macrophages treated by
755 edicotinib or U0126 (10 µM) or vehicle determined by RT-qPCR (n=3). Relative expression
756 compared to control macrophages in normoxia.

757 Supplementary Figure 4

758 (A) Immunoblot of CD206 in hypoxic macrophages co-cultured with tumors exposed to
759 edicotinib vs vehicle (DMSO) for 24h. Representative of three independent experiments.

760 (B) Gene expression of *CD206* and *CD38* genes in human macrophages treated by edicotinib
761 in hypoxia. Gene expression levels are expressed in FPKM=Fragments Per Kilobase Million.

762 Supplementary Figure 5

763 Flow cytometry analysis of sorted Monocytes, T lymphocytes and B lymphocytes using CD14,
764 CD3 and CD20 expression respectively. Representative of three independent experiments on
765 healthy donors.

Sexe	Age	Histologic diagnosis	Surgery	TNM	Molecular charactrization
F	92	Adenocarcinoma	Right colectomy (coelioscopic)	pT4N1R0	p-MMR
M	71	Adenocarcinoma poorly differentiated	Right colectomy (coelioscopic)	pT3N1R0	MSI (loss MSH6)
F	55	Adenocarcinoma poorly differentiated low grade	Sigmoidectomy	pT3N2bR0	NA
F	69	adenocarcinoma well differnetiated on tubulovillous adenoma	Left Colectomy	pT3pN1R0	pMMR
M	74	Adenocarcinoma (lieberkühnien)	Left Colectomy	pT3N0	MSS
F	70	Adenocarcinoma (lieberkühnien) low grade	Left colectomy	pT3N0M0	MMR
M	63	Adénocarcinoma low grade	Right colectomy (coelioscopic)	pT4N1b	MMR
M	84	Adenocarcinoma (lieberkühnien) low grade	Right colectomy (coelioscopic)	pT3N0R0	NA

Figure 1

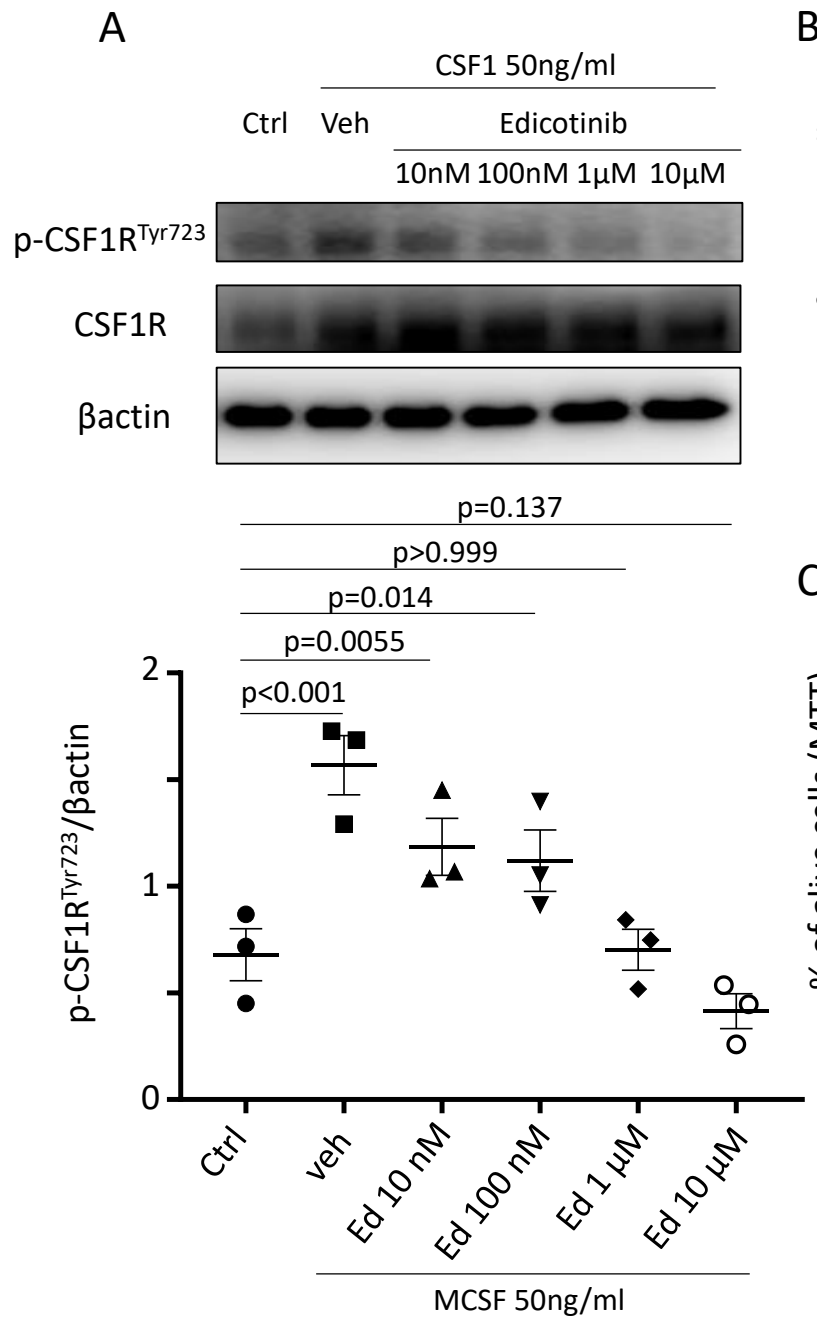
A
CSF1 50ng/ml
Ctrl
Veh
Edicotinib
10nM 100nM 1µM 10µM
p-CSF1R Tyr723
CSF1R
βactin
p=0.137
p>0.999
p=0.014
p=0.0055
p<0.001
p-CSF1R Tyr723/βactin
0
1
2
Ctrl
veh
Ed 10 nM
Ed 100 nM
Ed 1 µM
Ed 10 µM
MCSF 50ng/ml

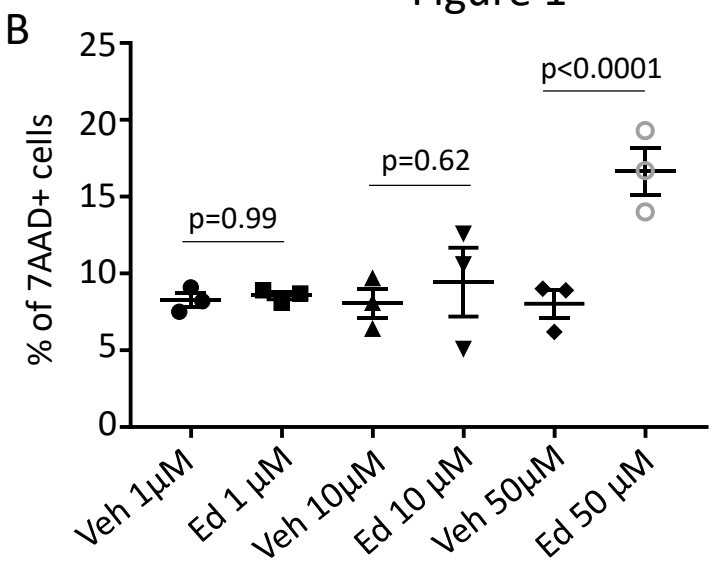
B
% of 7AAD+ cells
0
5
10
15
20
25
p=0.99
p=0.62
p<0.0001
Veh 1µM
Ed 1 µM
Veh 10µM
Ed 10 µM
Veh 50µM
Ed 50 µM

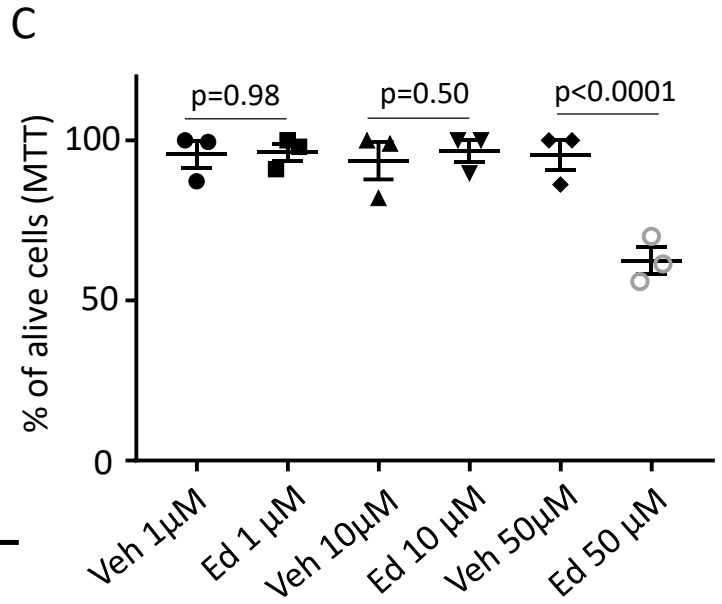
C
% of alive cells (MTT)
0
50
100
p=0.98
p=0.50
p<0.0001
Veh 1µM
Ed 1 µM
Veh 10µM
Ed 10 µM
Veh 50µM
Ed 50 µM

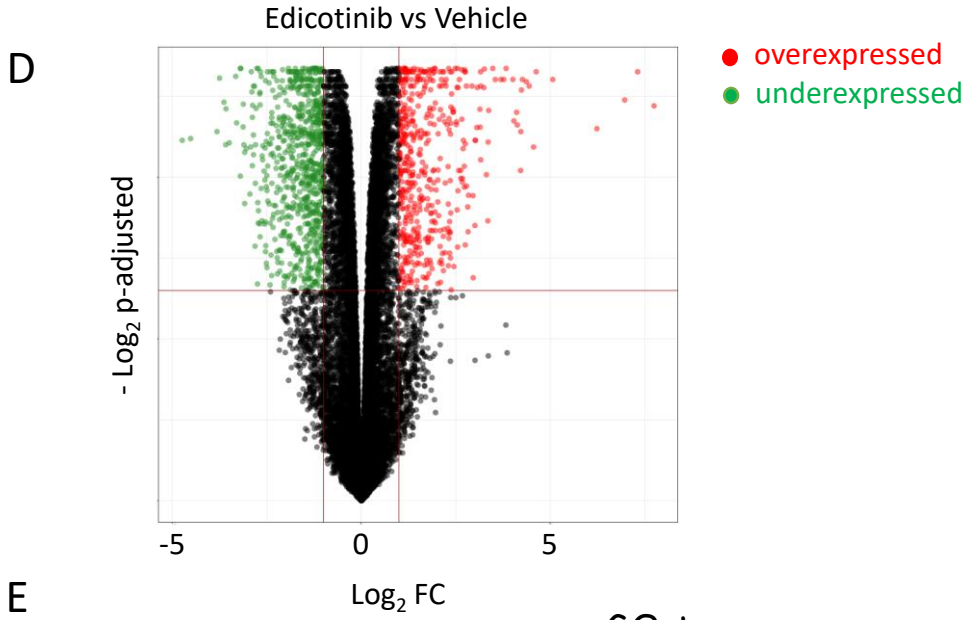
D
Edicotinib vs Vehicle
overexpressed
underexpressed
- Log2 p-adjusted
Log2 FC
-5
0
5

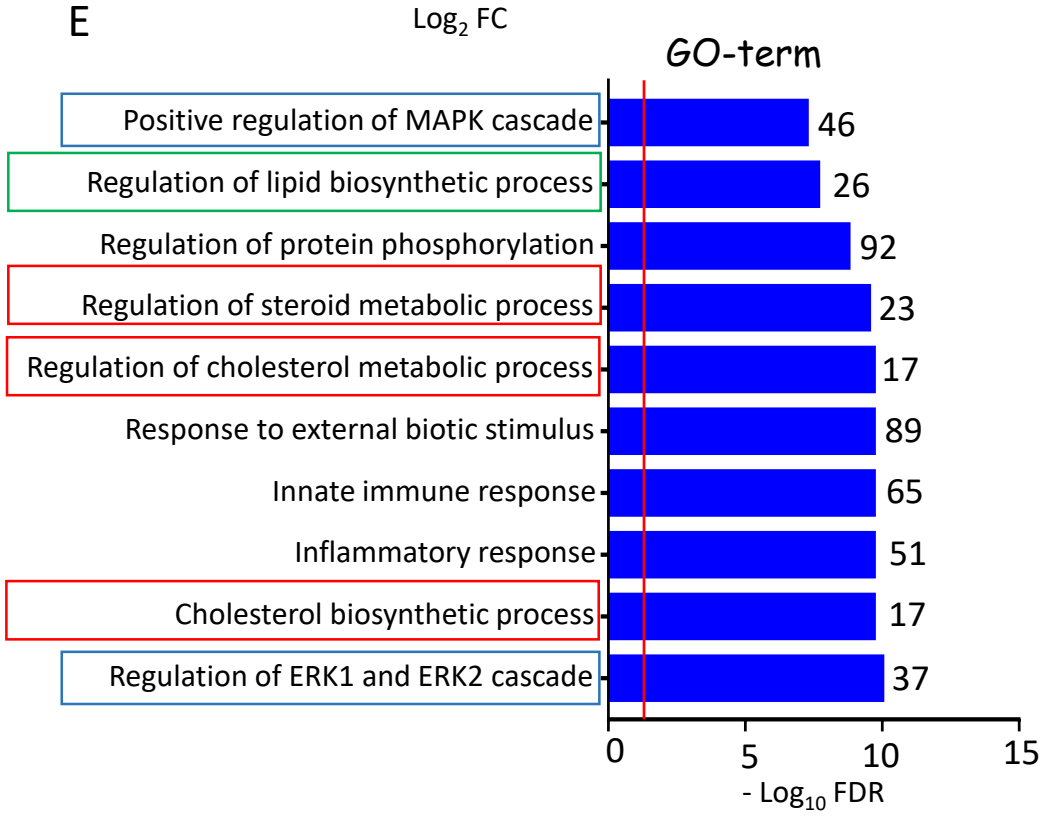
E
GO-term
Positive regulation of MAPK cascade 46
Regulation of lipid biosynthetic process 26
Regulation of protein phosphorylation 92
Regulation of steroid metabolic process 23
Regulation of cholesterol metabolic process 17
Response to external biotic stimulus 89
Innate immune response 65
Inflammatory response 51
Cholesterol biosynthetic process 17
Regulation of ERK1 and ERK2 cascade 37
0
5
10
15
- Log10 FDR

Supplemental Figure 1

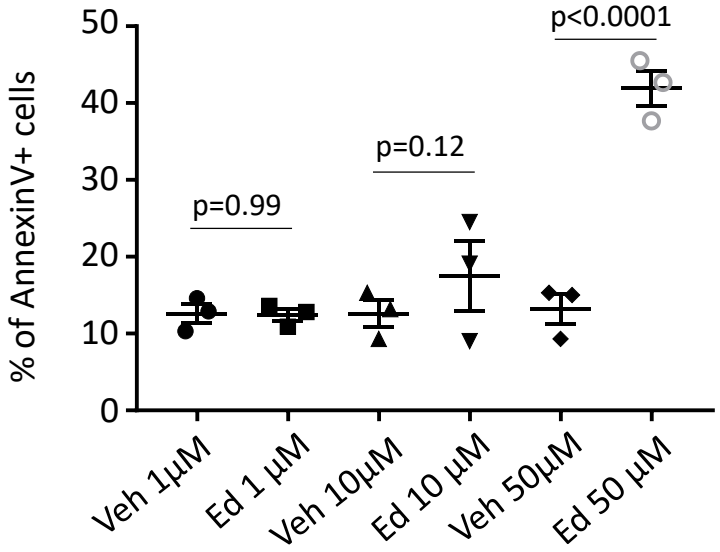

Figure 2

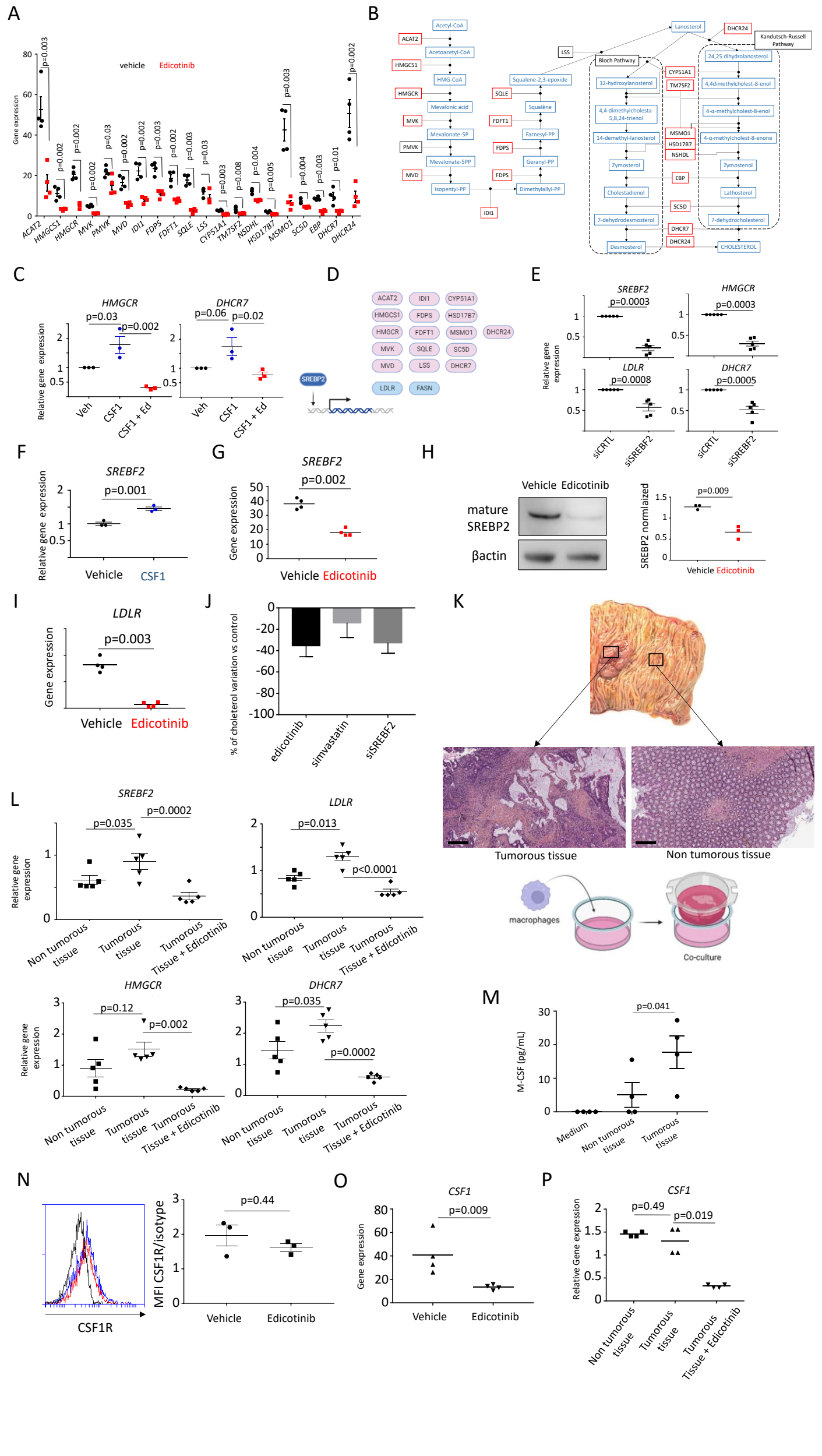
A
vehicle
Edicotinib
Gene expression
ACAT2
HMGCS1
HMGCR
MVK
PMVK
MVD
IDI1
FDPS
FDFT1
SQLE
LSS
CYP51A1
TM7SF2
NSDHL
HSD17B7
MSMO1
SC5D
EBP
DHCR7
DHCR24
B
Acetyl-CoA
Acetoacetyl-CoA
HMG-CoA
Mevalonic acid
Mevalonate-5P
Mevalonate-5PP
Isopentyl-PP
Dimethylallyl-PP
Geranyl-PP
Farnesyl-PP
Squalène
Squalene-2,3-epoxide
Lanosterol
Bloch Pathway
Kandutsch-Russell Pathway
32-hydroxylanosterol
4,4-dimethylcholesta-5,8,24-trienol
14-demethyl-lanosterol
Zymosterol
Cholestadienol
7-dehydrodesmosterol
Desmosterol
24,25 dihydrolanosterol
4,4dimethylcholest-8-enol
4-α-methylcholest-8-enol
4-α-methylcholest-8-enone
Zymostenol
Lathosterol
7-dehydrocholesterol
CHOLESTEROL
C
HMGCR
DHCR7
Relative gene expression
Veh
CSF1
CSF1 + Ed
D
SREBP2
E
SREBF2
HMGCR
LDLR
DHCR7
Relative gene expression
siCRTL
siSREBF2
F
SREBF2
Relative gene expression
Vehicle
CSF1
G
SREBF2
Gene expression
Vehicle
Edicotinib
H
Vehicle
Edicotinib
mature SREBP2
βactin
SREBP2 normalized
I
LDLR
Gene expression
Vehicle
Edicotinib
J
% of choleterol variation vs control
edicotinib
simvastatin
siSREBF2
K
Tumorous tissue
Non tumorous tissue
macrophages
Co-culture
L
SREBF2
LDLR
HMGCR
DHCR7
Relative gene expression
Non tumorous tissue
Tumorous tissue
Tumorous Tissue + Edicotinib
M
M-CSF (pg/mL)
Medium
Non tumorous tissue
Tumorous tissue
N
CSF1R
MFI CSF1R/isotype
Vehicle
Edicotinib
O
CSF1
Gene expression
Vehicle
Edicotinib
P
CSF1
Relative Gene expression
Non tumorous tissue
Tumorous tissue
Tumorous Tissue + Edicotinib

Supplemental Figure 2

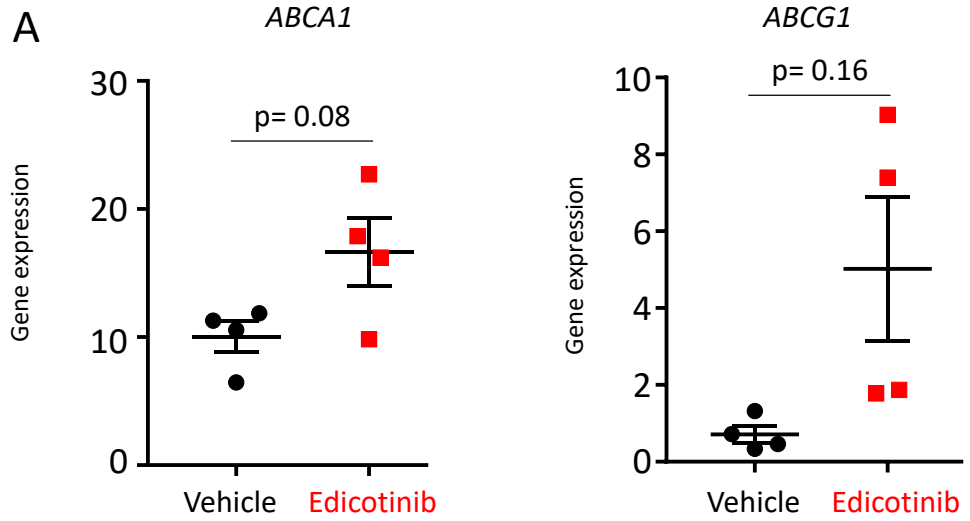

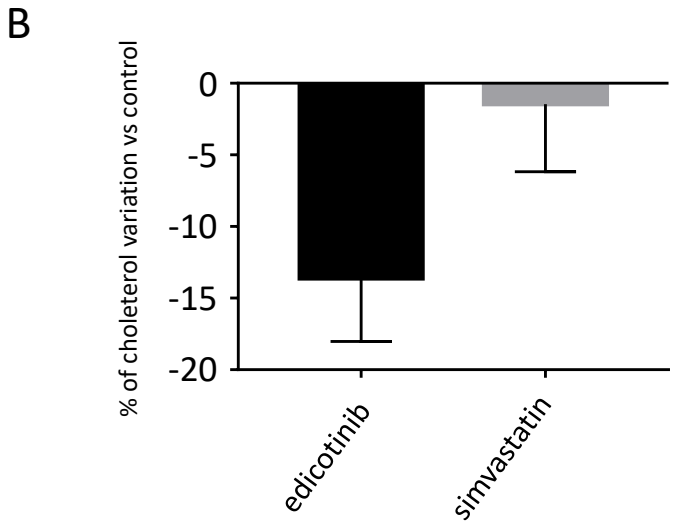

Figure 3

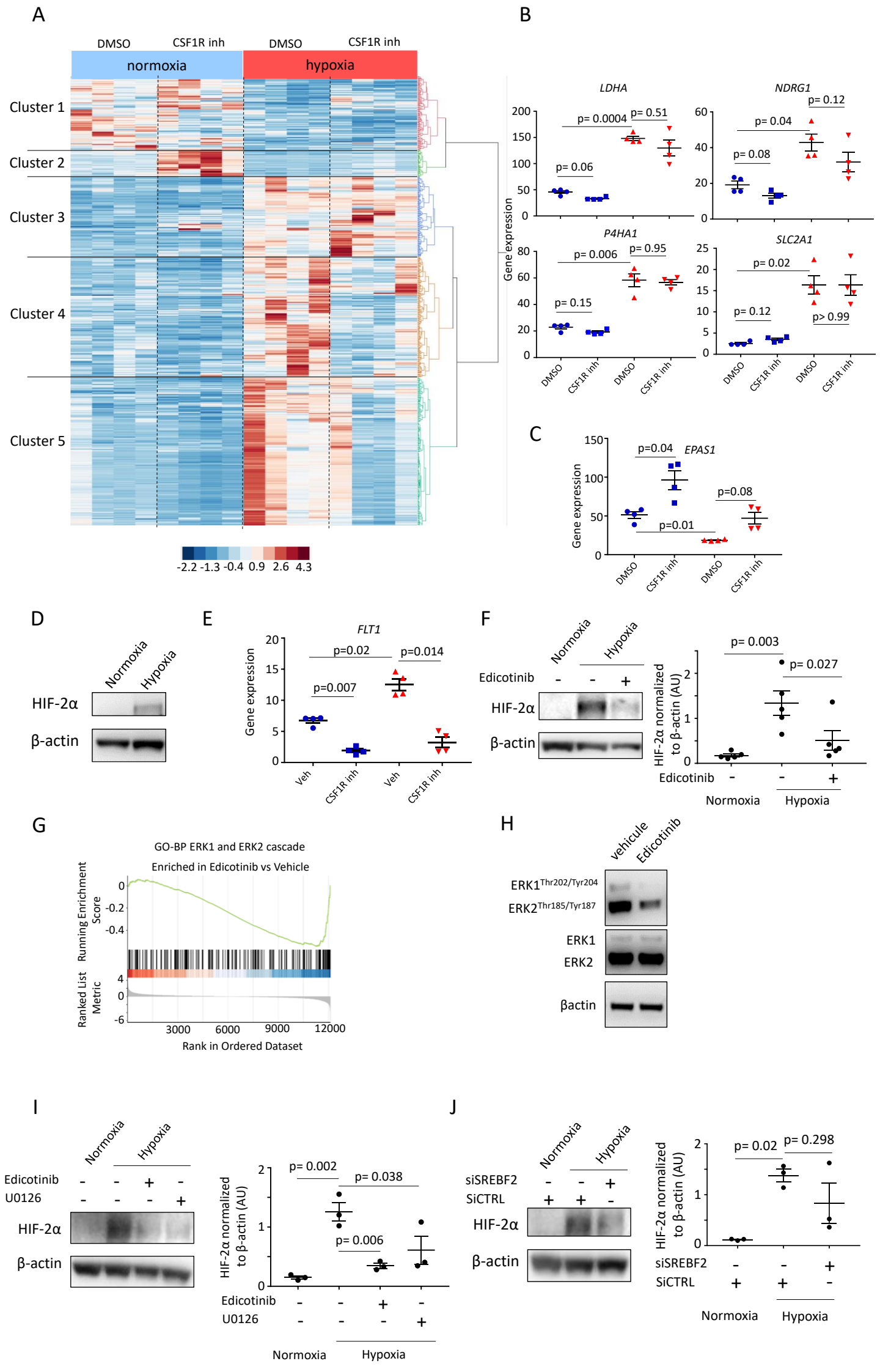
A
DMSO
CSF1R inh
DMSO
CSF1R inh
normoxia
hypoxia
Cluster 1
Cluster 2
Cluster 3
Cluster 4
Cluster 5
-2.2 -1.3 -0.4 0.9 2.6 4.3
B
LDHA
NDRG1
P4HA1
SLC2A1
Gene expression
p= 0.0004
p= 0.51
p= 0.06
p= 0.04
p= 0.12
p= 0.08
p= 0.006
p= 0.95
p= 0.15
p= 0.02
p= 0.12
p> 0.99
DMSO
CSF1R inh
DMSO
CSF1R inh
C
EPAS1
Gene expression
p=0.04
p=0.08
p=0.01
DMSO
CSF1R inh
DMSO
CSF1R inh
D
Normoxia
Hypoxia
HIF-2α
β-actin
E
FLT1
Gene expression
p=0.02
p=0.014
p=0.007
Veh
CSF1R inh
Veh
CSF1R inh
F
Normoxia
Hypoxia
Edicotinib
HIF-2α
β-actin
HIF-2α normalized to β-actin (AU)
p= 0.003
p= 0.027
Edicotinib
Normoxia
Hypoxia
G
GO-BP ERK1 and ERK2 cascade
Enriched in Edicotinib vs Vehicle
Running Enrichment Score
Ranked List Metric
Rank in Ordered Dataset
H
vehicule
Edicotinib
ERK1Thr202/Tyr204
ERK2Thr185/Tyr187
ERK1
ERK2
βactin
I
Normoxia
Hypoxia
Edicotinib
U0126
HIF-2α
β-actin
HIF-2α normalized to β-actin (AU)
p= 0.002
p= 0.038
p= 0.006
Edicotinib
U0126
Normoxia
Hypoxia
J
Normoxia
Hypoxia
siSREBF2
SiCTRL
HIF-2α
β-actin
HIF-2α normalized to β-actin (AU)
p= 0.02
p= 0.298
siSREBF2
SiCTRL
Normoxia
Hypoxia

Supplemental Figure 3

A

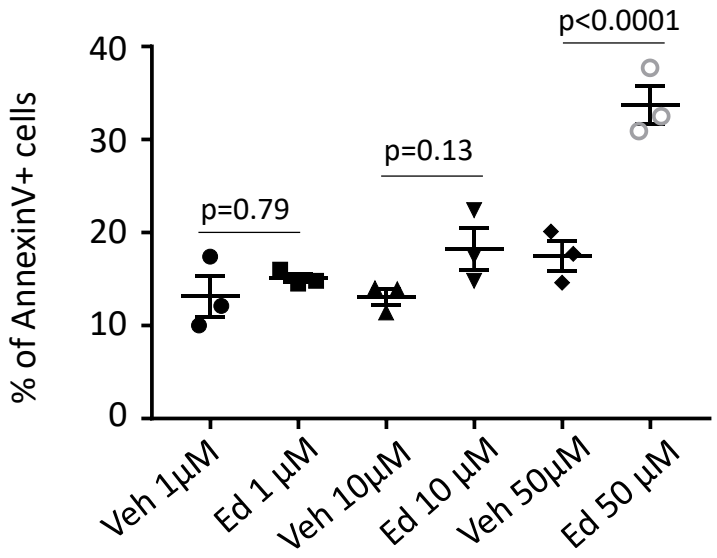

B

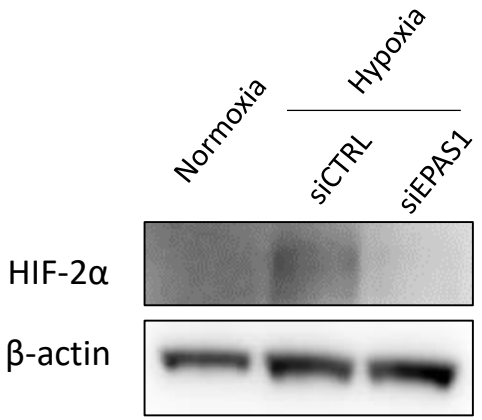

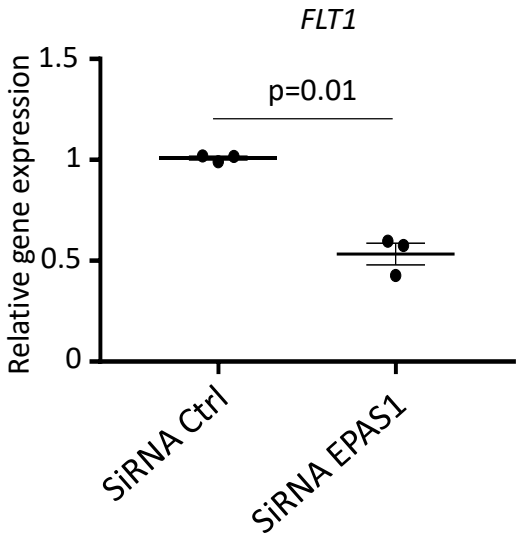

C

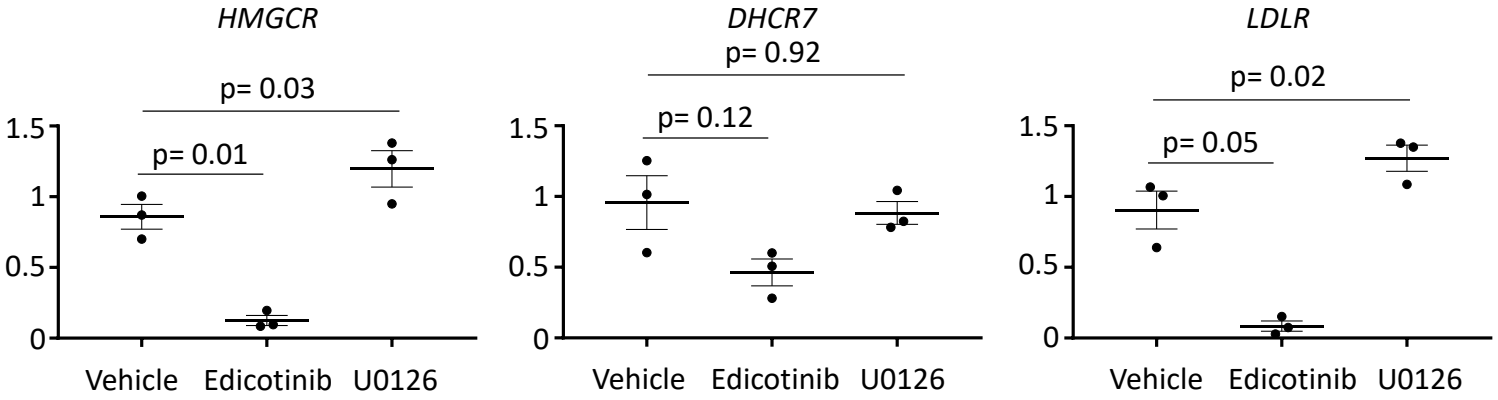

Figure 4

A

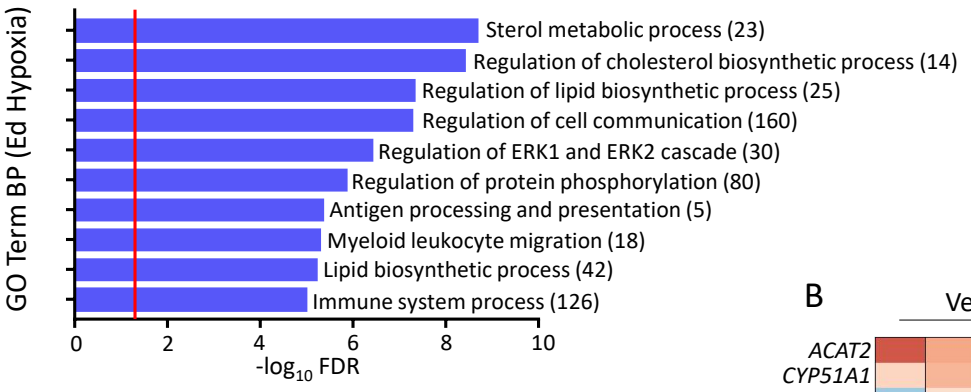

B

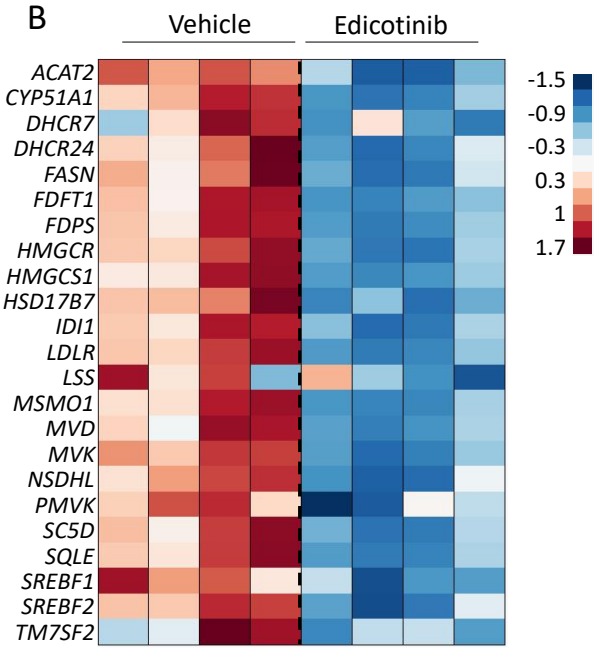

C

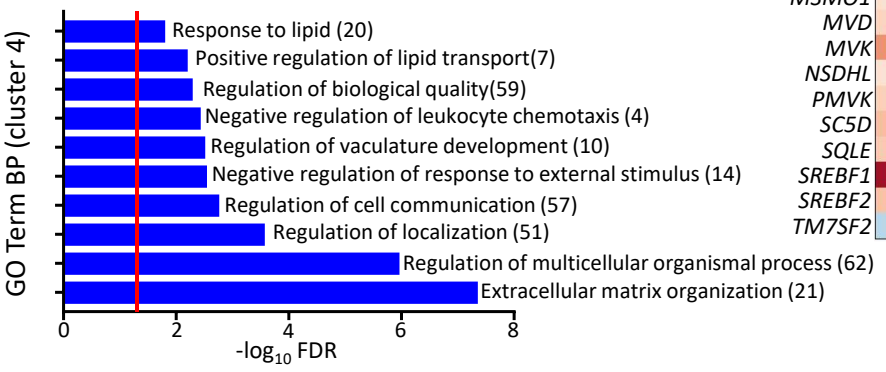

D

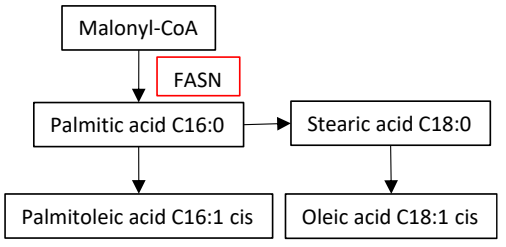

E

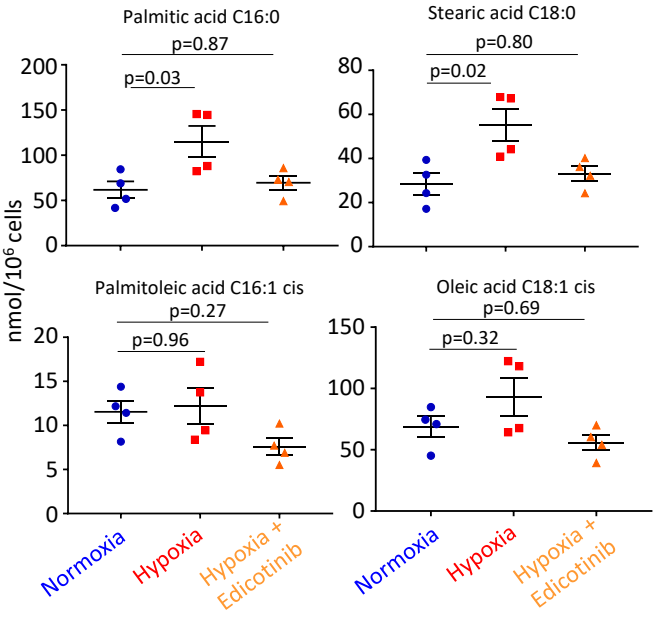

F

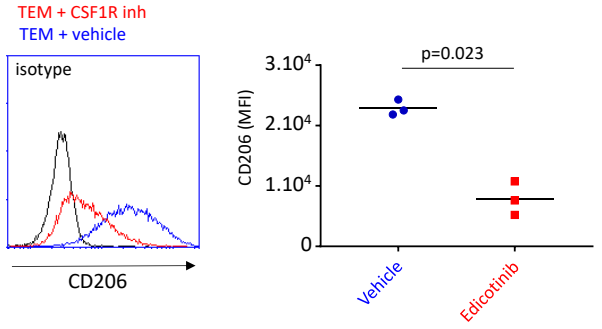

G

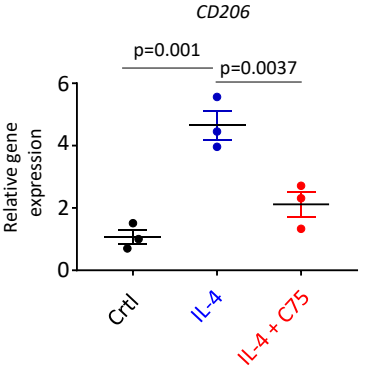

Supplemental Figure 4

A

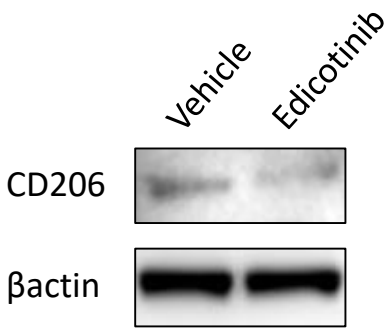

B

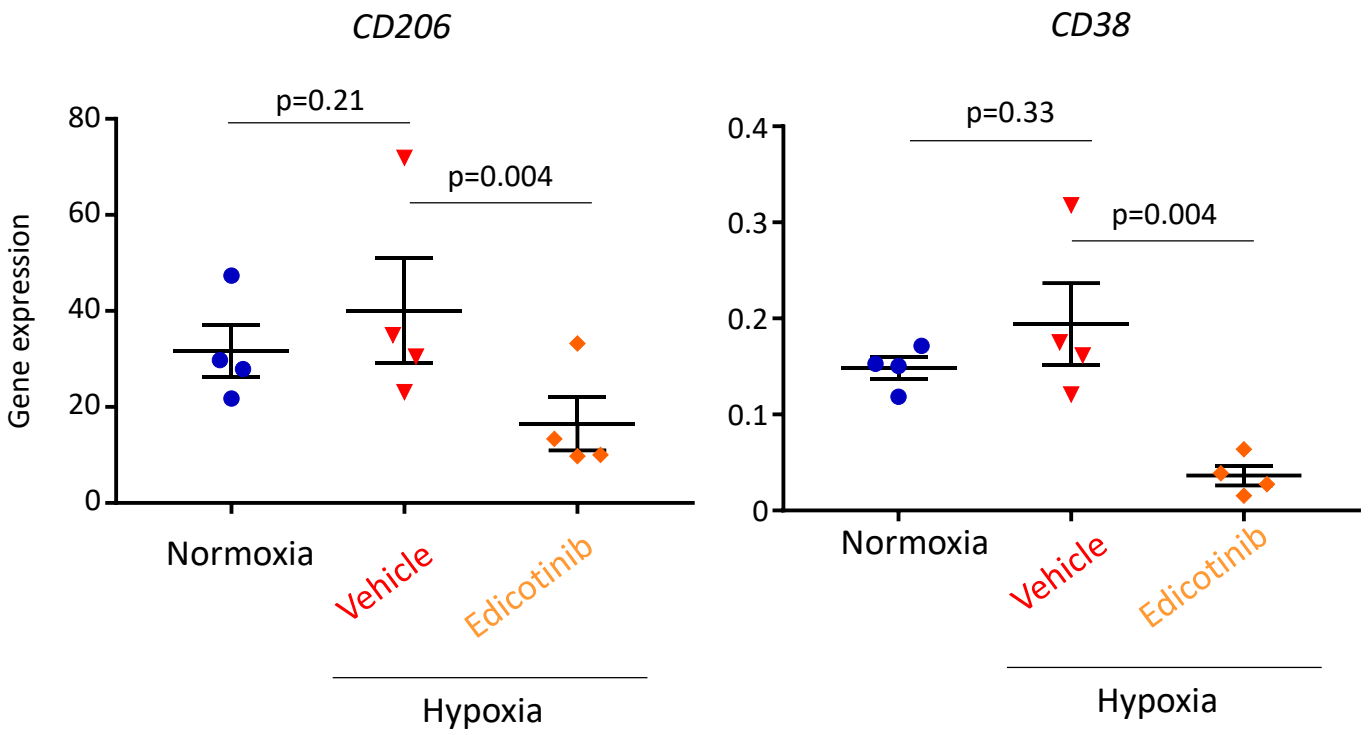

Figure 5

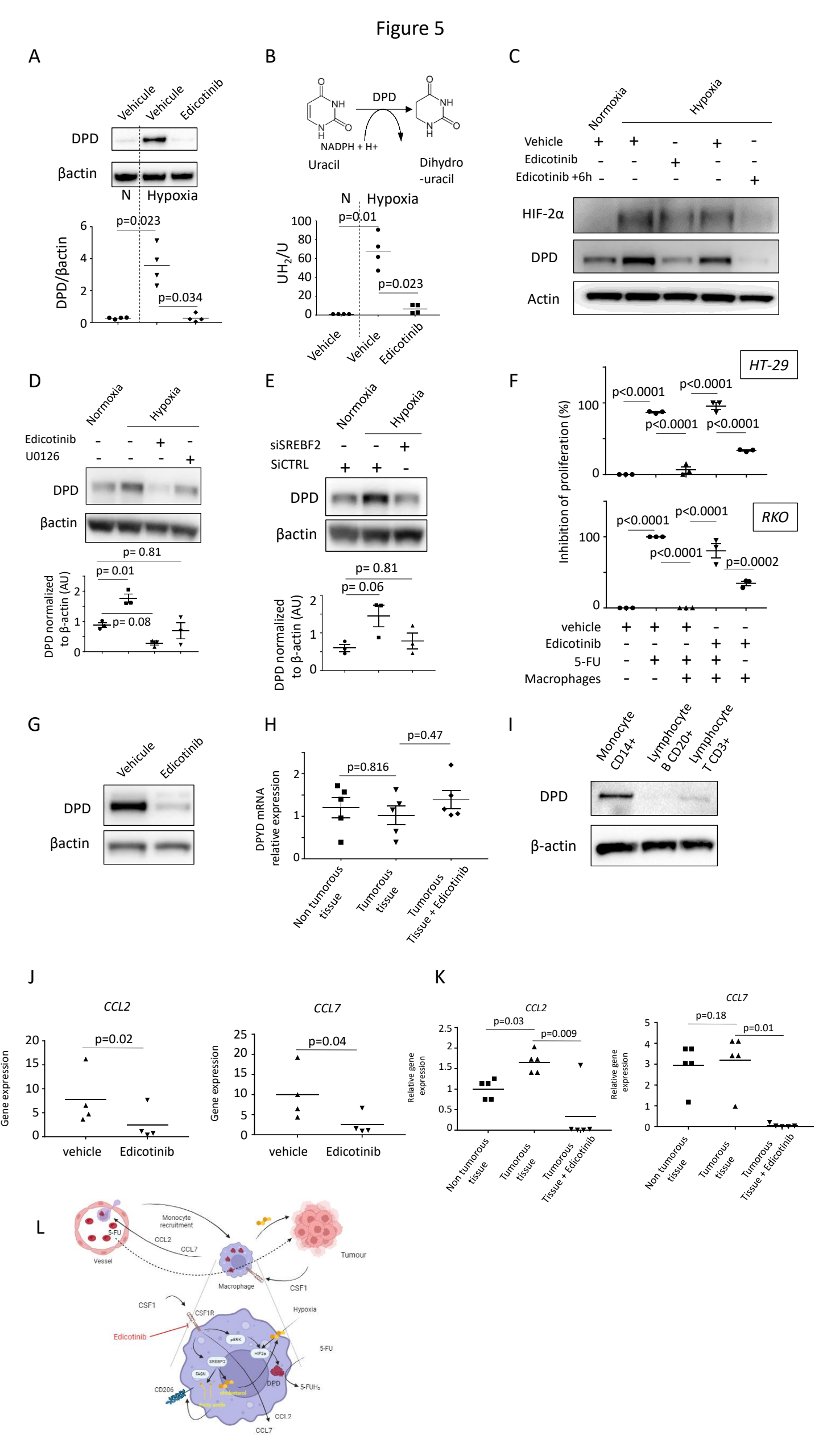
A
Vehicule
Vehicule
Edicotinib
DPD
βactin
N
Hypoxia
DPD/βactin
p=0.023
p=0.034
B
DPD
NADPH + H+
Uracil
Dihydro -uracil
N
Hypoxia
UH2/U
p=0.01
p=0.023
Vehicle
Vehicle
Edicotinib
C
Normoxia
Hypoxia
Vehicle
Edicotinib
Edicotinib +6h
HIF-2α
DPD
Actin
D
Normoxia
Hypoxia
Edicotinib
U0126
DPD
βactin
p= 0.81
p= 0.01
p= 0.08
DPD normalized to β-actin (AU)
E
Normoxia
Hypoxia
siSREBF2
SiCTRL
DPD
βactin
p= 0.81
p= 0.06
DPD normalized to β-actin (AU)
F
HT-29
RKO
Inhibition of proliferation (%)
p<0.0001
p<0.0001
p<0.0001
p<0.0001
p<0.0001
p<0.0001
p<0.0001
p=0.0002
vehicle
Edicotinib
5-FU
Macrophages
G
Vehicule
Edicotinib
DPD
βactin
H
p=0.47
p=0.816
DPYD mRNA relative expression
Non tumorous tissue
Tumorous tissue
Tumorous Tissue + Edicotinib
I
Monocyte CD14+
Lymphocyte B CD20+
Lymphocyte T CD3+
DPD
β-actin
J
CCL2
p=0.02
Gene expression
vehicle
Edicotinib
CCL7
p=0.04
Gene expression
vehicle
Edicotinib
K
CCL2
p=0.03
p=0.009
Relative gene expression
Non tumorous tissue
Tumorous tissue
Tumorous Tissue + Edicotinib
CCL7
p=0.18
p=0.01
Relative gene expression
Non tumorous tissue
Tumorous tissue
Tumorous Tissue + Edicotinib
L
Monocyte recruitment
5-FU
CCL2
CCL7
Vessel
Tumour
Macrophage
CSF1
CSF1
CSF1R
Hypoxia
Edicotinib
pERK
HIF2α
5-FU
SREBF2
FASN
DPD
5-FUH2
CD206
cholesterol
fatty acids
CCL2
CCL7
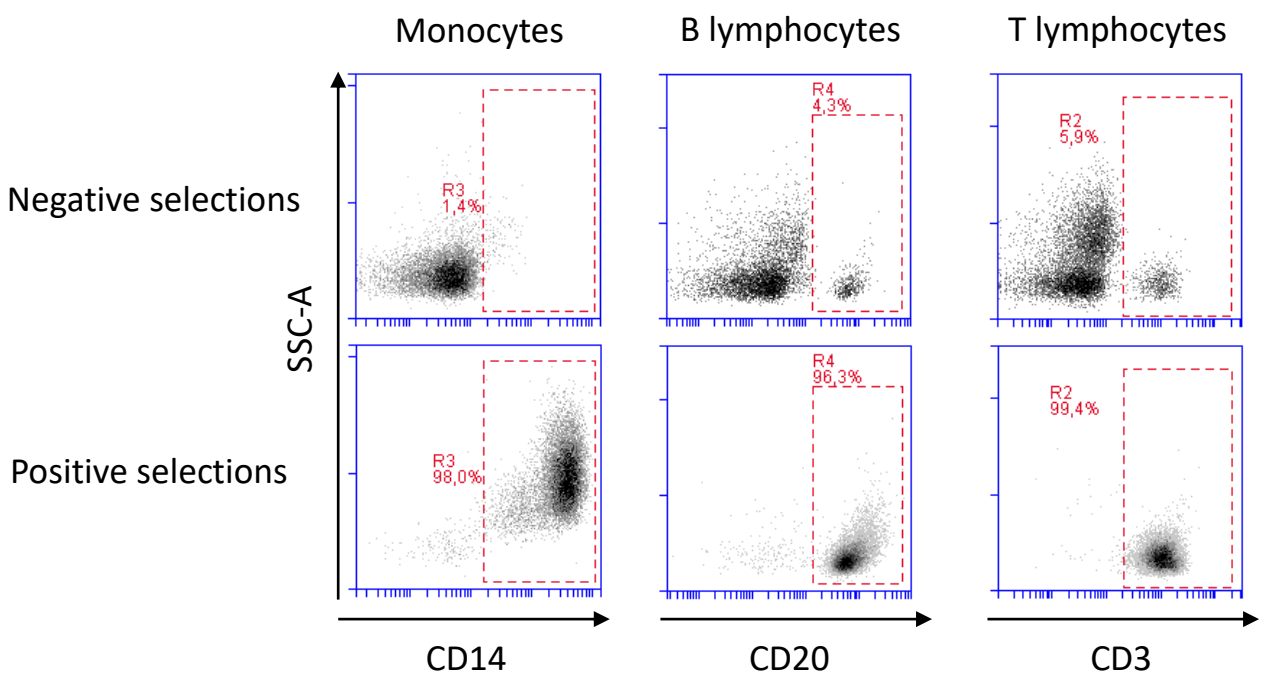
Supplemental figure 5